Chapter 4

Magnetic properties of nanostructures

Magnetism has fascinated mankind ever since the first reports, which date back to ancient China and Greece. The word derives from the greek word 'magnítis líthos' for lodestone (magnetite Fe_3O_4) from the area of Magnesia. Earliest reports date back to China, where magnetite has been used already in the 4th century BC as magnetic needles in compasses.

For the basic understanding of condensed matter, the spontaneous symmetry breaking and the related order parameter, i.e., the magnetization M, in addition to the structural order (usually the lattice), are very fundamental issues.

From the application perspective, famous examples are magnetic storage media or magnetic elements in transformers or electrical motors, just to name a few. While these may be considered "bulk" phenomena and applications, there are important and new effects when considering the nanoscale.

Nanomagnetism is concerned with the magnetic properties of systems which are reduced, at least in one dimension, to sizes of typically $< 100\,\mathrm{nm}$, such that the behavior deviates from that of their macroscopic counterparts. These are thin films and multilayers (heterostructures), as well as magnetic nanoparticles (MNPs), single molecule magnets (SMMs), nanodots and nanowires, including macroscopic samples with ensembles of these. In most cases we will consider materials which in the bulk display ferromagnetism or ferrimagnetism, i.e. exhibit a spontaneous magnetization.

Nanomagnetism exhibits a multitude of practical **applications** in very different areas:

- Geology: MNPs in rocks and the soil. Their alignment allows to draw conclusions on the evolution of the earth's magnetic field, and the determination of the age of samples.
- Biology: MNPs – typically magnetite – in living organisms, in particular magnetotactic bacteria or birds for the purpose of navigation.
- Magnetic data storage: The quest for steadily increasing storage density based on magnetic materials initially was the major driver for the technological development of MNPs and research on their properties, which may significantly deviate

from bulk magnetic materials. This has led to a revolutionary development of the storage densities. It has also opened up the area of spintronics exploiting the electron as a carrier of charge **and** spin.

- Ferrofluidics: MNPs immersed in a suitable carrier fluid with interesting applications, including loudspeakers.
- Biomedical applications: e.g. cell labeling (for imaging) and separation, targeted drug delivery to specific organs or tissue and cancer treatment (magnetic hyperthermia).
- Quantum information processing: More recently, significant efforts have been devoted to exploit quantum mechanical properties of MNPs and in particular SMMs as the basic building blocks (quantum bits) for quantum processors.

Will first start with a brief recap of some basics of magnetism in the bulk as a starting point (Sec. 4.1). After that we will discuss what is expected to be different from a general perspective on the nanoscale, with relevant length scales and comments on the density of states in reduced dimensions (Sec. 4.2). These have an impact on a number of fundamental issues, including the magnetic ordering transition (ferromagnetic – paramagnetic) itself. This chapter continues with micromagnetic modelling and the various contributions to the energy of the magnetization as well as with magnetic domains (Sec. 4.3). Magnetic nanoparticles and other nano-objects are covered in Sec. 4.4. Section 4.5 discusses magnetic thin films and multilayers, including the very important topic of magnetic storage and magnetic transport.

While we hope that this chapter provides the basics of nano-magnetism, a detailed discussion of further advanced topics, although tempting, is beyond the scope of this course. The interested reader is referred to the list of original literature (Sec. 5.6) as well as suggestions for further reading on a more advanced level (Sec. 4.7).

4.1 Recap of Magnetism in the Bulk

There are various forms of magnetism, categorized depending on the response of the system to an external field H. Diamagnetic and paramagnetic systems exhibit no magnetic order for vanishing H. In this chapter, we shall concentrate on ferromagnetic systems, which implicitly also include antiferromagnetism and ferrimagnetism and other forms of (permanent) magnetic order, unless stated otherwise.

For permanent magnetism, the key interaction is the exchange interaction, which in essence goes back to Pauli's exclusion principle and the anti-symmetrization of the total wavefunction of electrons. Ferromagnetism is thus inherently a quantum mechanical phenomenon. Note that there are many variants of exchange interactions, including the interaction which can oscillate in sign between two layers (similar to the RKKY interaction; see Sec. 4.5.2).

In addition to the exchange interaction, there can be various other contributions to the total energy of the system, including, e.g., shape anisotropy and magnetocrystalline anisotropy. This is essential for the understanding of $M(H)$ hysteresis loops, which are technologically very important. For nano-structured systems, of course, the large surface-to-volume ratio has to be considered, and also surface-related terms enter (see Sec. 4.3).

For the temperature dependence of the magnetization $M(T)$, spinwave theory gives the Bloch $T^{3/2}$ law for the reduction of M with increasing T at low T for a bulk ferromagnet. This is inherently related to the density of states in three dimensions (3D). Therefore, and also due to the existence of surfaces and generally the finite size of the sample, significant changes of $M(T)$ in general and in particular of the phase transition behavior occur.

When atoms are combined to form a crystal, the overlap of their wavefunctions leads to a delocalization of the electrons, which lowers their kinetic energy. This affects in particular the outer s- and p- valence electrons, but also the 3d-electrons. The hybridization of electron orbitals leads to the formation of energy bands in the solid. This significantly modifies the occupation of spin and orbital momentum states of electrons, which are linked to the magnetic moment, and which for single atoms is governed by Hund's rules. As a consequence, the magnetic moments per atom are usually reduced in a solid, as compared to the moments in single atoms.

Finally, we note that in particular in the area of magnetism the coexistence of different notations, conventions and units can be confusing. Unless stated otherwise, we will use SI units and conventions in this chapter.

4.2 What is Different in Nanomagnetism?

4.2.1 Why is the nm-Scale so Important in Magnetism?

Two reasons:
i) for $\lesssim$100 nm, fundamental properties are different than in the bulk
ii) these fundamental properties depend on sample size

What makes the difference in the magnetic properties of nm-sized samples as compared to macroscopic systems?

- The size of nanoobjects is comparable to some fundamental **characteristic lengths** of the material. Important for magnetic properties are e.g. the exchange length l_{ex}, the domain wall width δ_0, the critical single-domain size D_{cr} and the spin diffusion length l_{sd}. Some of these characteristic lengths are listed in Tab. 4.1, together with their typical magnitudes. Obviously, magnetic nanosystems have sizes which fall into the range of many of those characteristic length scales

  Simplest example for the impact of characteristic length scales on MNPs:
  Sample size is smaller than the critical size of a single magnetic domain (critical single-domain size D_{cr})
  $\Rightarrow$ a single-domain state is the configuration of lowest energy.

Table 4.1: Characteristic lengths and their typical magnitude; from [Guimarães, 2009].

Symbol	length	magnitude (nm)
d_a	interatomic distance (Fe)	0.25
d_{ex}	range of exchange interaction	$0.1 - 1$
d_{RKKY}	range of RKKY interaction	$0.1 - 10$
d_c	domain size	$10 - 10^4$
D_{cr}	critical single-domain size	$10 - 10^3$
D_{sp}	superparamagnetic critical diameter	1–100
δ_0	domain wall width	1–100
l_{ex}	exchange length	1-100
l_{sd}	spin diffusion length	10–100
l_e	electronic mean free path	1–100
ξ	superconductor coherence length	1–1000
λ_F	Fermi wavelength metal (semiconductor)	0.1 (100)

- Broken translation symmetry at surfaces and interfaces:
  Lattice sites with reduced coordination number and with modified or broken (exchange) bonds $\Rightarrow$ structural & orbital reconstruction
  $\rightarrow$ modified elektronic density of states (see below) and frustration effects in the magnetic order
  $\rightarrow$ strong dependence on the environment
  (e.g. substrate or cover laver in thin films)
  $\rightarrow$ Effects become more pronounced with shrinking size
  (increasing portion of atoms at the surface and interface)

- Electronic density of states:
  i) In metallic nm-sized particles, the energy difference betwen quantum states of the conduction electrons becomes significant, in comparison to other energies, e.g. thermal energy or Zeeman energy.
  Free electron gas:
  $\Delta k = 2\pi/L \rightarrow \Delta E = (\hbar\Delta k)^2/2m = (h/L)^2/2m \approx 1.5\,e\mathrm{V}/L^2(\mathrm{nm}^2)$

  ii) Electronic densities of states (vs energy) – and hence also the magnetic properties – depend on the dimensionality of the system

  iii) Typically, the magnetic moment per atom in MNPs increases with decreasing number of atoms (particle size), which is associated with the narrowing of the energy bands.

- Modified excitation spectrum of spin waves:
  Thermally excited spin wave ($k_BT \approx E_{sw}$) with $E_{sw} = \hbar\omega_{sw} = D_{sw}k_{sw}^2$
  $\rightarrow k_{sw} \approx \sqrt{k_BT/D_{sw}} \approx 1/3\,\mathrm{nm}$ ($T = 4.2\,\mathrm{K}$, $D_{sw} \sim 3\,\mathrm{meV\,nm}^2$) $\rightarrow \lambda_{sw} \sim 20\,\mathrm{nm}$.
  Spin wave excitations are modfied when the sample size reaches the order of λ_{sw}.

- Modified dynamic properties, in particular magnetization reversal of MNPs:
  The dynamic behavior of the magnetization of nanomagnets changes significantly with shrinking sample size. On the one hand, the magnetization reversal ($M(H)$ hysteresis loops) for multi- and mono-domain systems is different. On the other hand, thermal fluctuations become increasingly important with shrinking sample size. This leads e.g. in MNPs to 'superparamagnetism': When the thermal energy k_BT bcomes comparable to the anisotropy energy (scales with the sample volume), the magnetization can spontaneously reverse due to thermal activation. This process can be observed above the so-called 'blocking temperature' T_B and has important consequences for applications. In particular, for magnetic data storage, this effect has to be considered within the advancing miniaturization of storage bits.

- The smaller the systems, the stronger is the impact of defects
  $\rightarrow$ practical problem for the analysis of ensembles of MNPs
  (dispersion with particle size)

4.2.2 Dimensionality and Phase Transitions

The change in behavior of a ferromagnet for reduced dimensions is also found for the phase transition. This is obviously a very fundamental subject with far-reaching implications. Its in-depth discussion is also rather involved and connected to the work of the 2016 Nobel laureates in physics, J. Michael Kosterlitz, F. Duncan M. Haldane, and David J. Thouless, amongst others (see also [ILL, 2016]).

We shall distinguish here two issues related to the change of the phase transition. The first (i) concerns the *absolute value* of the Curie temperature T_C, i.e. for a thin film with thickness d_f the question of $T_\mathrm{C} = T_\mathrm{C}(d_f)$ and, in fact, the question of the very existence of the phase transition, meaning whether or not there is a ferromagnetic phase at all for a thin film. The second (ii) is related to a possible change of the *nature*

of the transition, i.e. for a given T_C whether or not the transition is, e.g., sharper or less sharp, which could be reflected in a change of critical exponents.

(i) Absolute value of T_C

We first consider the question of the existence of a ferromagnetic phase. It was first pointed out by Mermin and Wagner [Mermin and Wagner, 1966] that at any non-zero temperature, a one- or two-dimensional isotropic spin-S Heisenberg model with finite-range exchange interaction can be neither ferromagnetic nor antiferromagnetic. The physical reason is that spinwave excitations (which in 3D lead to the Bloch $T^{3/2}$ law) become infinitely easy, i.e. the magnetization reduction due to magnons diverges and at any finite T they destroy ferromagnetic order.

Comparison with experiments on real-world samples

It is important to bear in mind the assumptions underlying the Mermin-Wagner-theorem. As soon as these are not fulfilled, ferromagnetic order is no longer prohibited. As the assumptions (isotropic and short-range) are usually not strictly fulfilled, it is hard to confirm Mermin-Wagner in a real system. Nevertheless, the theorem provides an important benchmark and gives a qualitative explanation why the ordering temperature T_C is usually reduced for thinner films.

Intuitively, we expect that a thin film of finite thickness d_f corresponding to, say, a few atomic layers, is somewhere between the Mermin-Wagner case and the bulk T_C of this element. In fact, this can be found in experiments, as shown in Ref. [Schneider et al., 1990] with a $T_C = T_C(d_f)$.

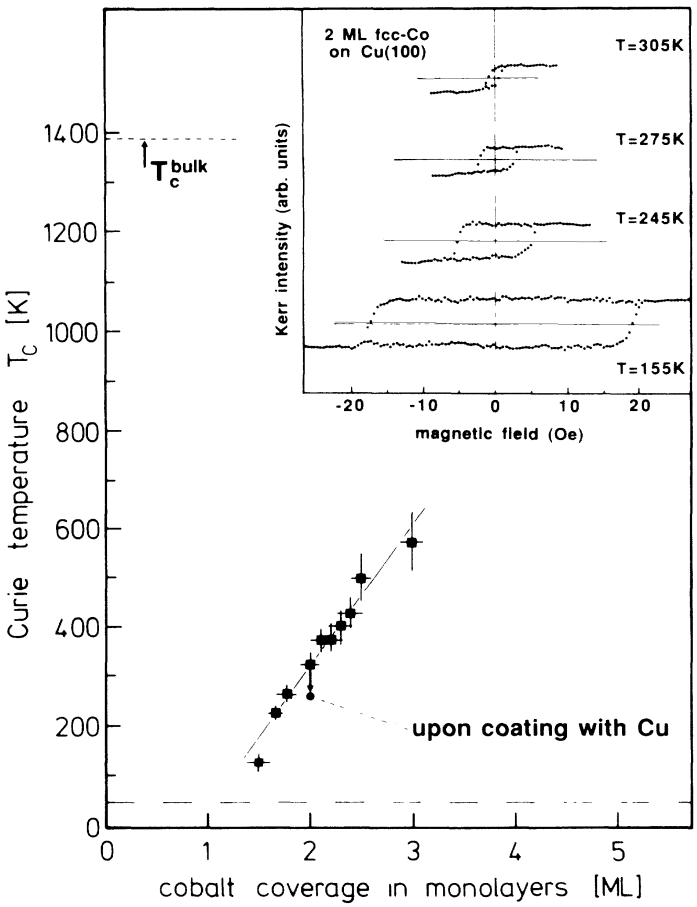

Fig. 4.1: Coverage dependence of the Curie temperature of fcc-Co films as determined from surface magneto-optical Kerr effect (SMOKE) experiments (the thin line serves to guide the eye). Inset: Variation of the hysteresis loop of a 2 monolayers (ML) thick film with sample temperature. This temperature dependence has been used to determine $T_C(d_f)$; from [Schneider et al., 1990].

(ii) Nature of the transition

Considering the nature of the transition, we recall that typically we find characteristic power laws for the relevant quantities near T_C. The change of magnetic properties in nanosystems as a function of dimensionality is also reflected in the critical exponents, which enter into the description of the divergence close to the transition temperature. Measurements on ferromagnetic systems close to the Curie temperature T_C reveal that the scaling of the specific heat C, the saturation magnetization M_s, the magnetic susceptibility χ are described by power laws:

$$\begin{aligned} C &\sim |T - T_C|^{-\alpha} \\ M_s &\sim |T_C - T|^{\beta} \\ \chi &\sim |T - T_C|^{-\gamma} \end{aligned} \tag{4.1}$$

Experimentally determined values for the critical exponentens of different magnetic systems are $\alpha \sim 0$, $\beta \sim 0.3$ und $\gamma \sim 1 - 2$.

Measurements of the magnetization as a function of temperature T for the determination of critical exponents in mesoscopic and nanoscopic systems allow for the experimental investigation of the dimensionality of such systems, as a function of their size (diameter, length, thickness, etc.). For example, this enabled the observation of the transition from 2D to 3D behavior in thin films (see Fig. 4.2).

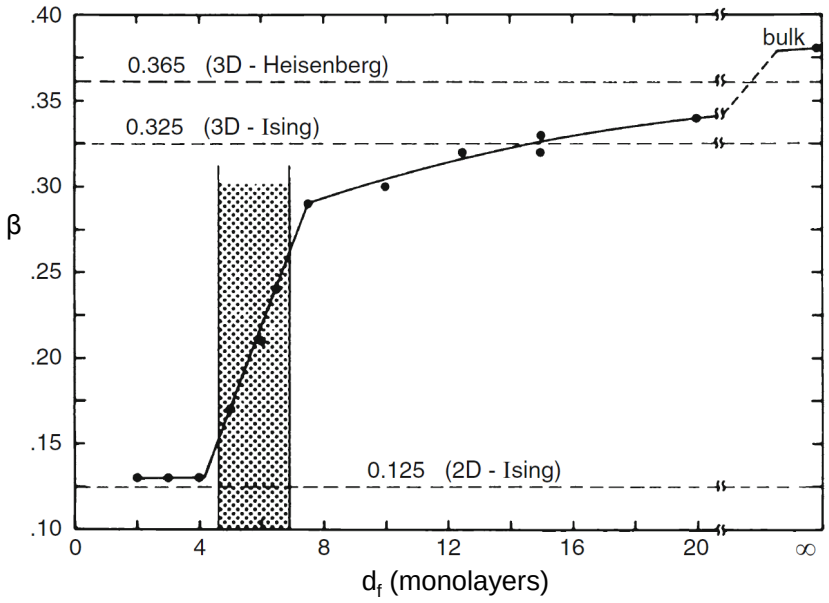

Fig. 4.2: Critcal exponent β vs film thickness d_f (in units of monolayers) in Ni(111) films on W(110); from [Guimarães, 2009].

However, the clear experimental proof of the impact of the change of dimensionality on the magnetic properties in nanosytems is not an easy task. This is due to the fact that sample inhomogenities (morphology, defects, ...) on the nm scala can also have a strong impact.

4.3 Micromagnetic Model & Magnetic Domains

If one reduces the size of a magnetic system, the first 'size-effect' emerges if the size of the particle becomes too small to form magnetic domains (areas with uniform magnetization). A treatment of this effect requires an understanding of the formation of domains which occurs in macroscopic systems. This means, one should understand the formation of homogeneously magnetized areas with different directions of magnetization for different domains.

The existence of magnetic domains is mainly based on the interplay between the exchange interaction, the magnetic anisotropy and the magnetostatic dipole interaction. In the following we present a model which describes these different contributions. From this model we can derive some already mentioned characteristic quantities (energies and lengths), which relate the different contributions.

4.3.1 Micromagnetic Model

The formation of domain structures is usually described within a micromagnetic model that stems from William F. Brown [Brown, 1940, Brown, 1963]. This classical, phenomenological model considers the different relevant energy contributions. Within this model, it is assumed that the material locally always reaches the saturation magnetization M_s, i.e. $|\boldsymbol{M}| = M_s$. Still, the orientation of $\boldsymbol{M}$ may vary spatially within the sample.

The starting point to find the configuration of the magnetization in thermodynamic equilibrium is the total energy

$$E_{tot}(\boldsymbol{H}_{ext}, \boldsymbol{M}) = U(\boldsymbol{M}) - \int \mu_0 \boldsymbol{H}_{ext} \cdot \boldsymbol{M} \, \mathrm{d}V \quad , \tag{4.2}$$

where U is the internal energy.[1] An equilibrium state (configuration of the magnetization) can be calculated by minimizing E_{tot}. In doing so, various intrinsic and extrinsic terms are considered:

$$E_{tot} = \underbrace{E_Z}_{\text{Zeeman energy}} + \underbrace{E_{ex}}_{exchange\,energy} + \underbrace{E_{ms}}_{magnetostatic\,energy} + \underbrace{E_A}_{anisotropy\,energy} \tag{4.3}$$

A. Zeeman energy

The Zeeman energy

$$E_Z = -\mu_0 \int \boldsymbol{H}_{ext} \cdot \boldsymbol{M} \, \mathrm{d}V \quad , \tag{4.4}$$

favours the orientation of the magnetic moments along the direction of the external field $\boldsymbol{H}_{ext}$. Here, the Zeeman energy density $e_Z = -\mu_0 \boldsymbol{H}_{ext} \cdot \boldsymbol{M}$ has to be integrated over the sample volume V.

[1] If one considers a dependence of the internal energy U on the magnetization $\boldsymbol{M}$, one can also describe the formation of metastable states.

B. Exchange energy

In the classical description of the Heisenberg model, the exchange energy between two spins $\boldsymbol{S}_i$, $\boldsymbol{S}_j$ is given by $E_{ex,ij} = -2J\boldsymbol{S}_i \cdot \boldsymbol{S}_j$, with the exchange constant $J > 0$ for ferromagnetic systems. The crossover to a continuum theory within the frame of the micromagnetic model is illustrated in Fig. 4.3. With the tilt angle $\Theta(i,j) = \Delta\Theta$

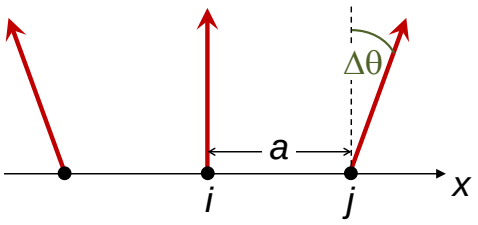

Fig. 4.3: Spins in a one dimensional chain with lattice constant a. Adjacent spins are tilted by the angle $\Delta\Theta$.

between two adjacent spins i and j (with $|\boldsymbol{S}_i| = |\boldsymbol{S}_j| = S$), that are separated by the distance a (lattice constant), the classical approximation yields

$$E_{ex,ij} = -2JS^2\cos(\Delta\Theta) \approx -2JS^2\left[1 - \frac{(\Delta\Theta)^2}{2}\right] = const. + JS^2a^2\left(\frac{\partial\Theta}{\partial x}\right)^2 \quad . \tag{4.5}$$

Here the approximation of small tilts was assumed; the rightmost term corresponds to the crossover ($\Delta\Theta \to a\,\partial\Theta/\partial x$) to a continuum model.

The exchange energy favors a long-range order of the spins. However, due to the very short-range exchange interaction, in most cases only the interaction between adjacent spins has to be taken into account. Starting from the mean field approximation [2], and extending the description to the three-dimensional case [3] one finds for the exchange energy density $e_{ex} = A(\nabla\boldsymbol{M})^2/M_s$, and by integration over the sample volume the exchange energy [4]

$$E_{ex} = \frac{A}{M_s^2}\int (\nabla\boldsymbol{M})^2\,\mathrm{d}V \quad . \tag{4.6}$$

Here, A is the (spatially homogeneous) **exchange stiffness constant** (typical values: 10^{-11} J/m), and M_s is the saturation magnetization. For a cubic lattice one finds

$$A = nJS^2/a \quad , \tag{4.7}$$

with $n = 1$ for a simple cubic lattice ($n = 2$ for a bcc, and $n = 3$ for a fcc lattice). The exchange stiffness constant A quantifies how difficult it is for a single magnetic moment to deviate from the direction of the exchange field $\boldsymbol{B}_{ex}$.

The term $(\nabla\boldsymbol{M})^2$ in (4.6) is defined as the sum of the squares of the gradient of the magnetization components M_x, M_y, M_z, i.e.

$$(\nabla\boldsymbol{M})^2 = \sum_{i=x,y,z}(\nabla M_i)^2 = \sum_{i,j=x,y,z}\left(\frac{\partial M_i}{\partial j}\right)^2 . \tag{4.8}$$

[2] There the exchange energy is considered as a Zeeman energy $E_{ex} = -\boldsymbol{\mu}\cdot\boldsymbol{B}_{ex}$ of the magnetic moment $\boldsymbol{\mu}$ in the effective exchange field $\boldsymbol{B}_{ex} = \lambda_m\mu_0\boldsymbol{M}$, where λ_m is the mean-field constant.

[3] An explicit description of the transition to 3D can, e.g., be found in [Guimarães, 2009].

[4] In Eq. (4.6) one simply neglegts the constant term in the r.h.s. of Eq. (4.5), i.e., the energetically most favorable homogeneous case has zero energy, and any deviation from that case increases the energy of the system.

Hence, the exchange energy inreases with the gradient of the magnetization, and it is minimum (=0) for a spatially homogeneous magnetization.

C. Magnetostatic (self-field) energy

The magnetostatic self-energy E_{ms} (dipolar energy, stray-field energy) results from the interaction of the magnetization of the system with the demagnetization magnetic field $\boldsymbol{H}_d$ that is induced by itself (integration over the dipole-dipole-interaction of the single moments). Using the Maxwell equation $\nabla \cdot \boldsymbol{B} = 0$, $\boldsymbol{H}_d$ follows from the divergence of the magnetization. Using $\boldsymbol{B} = \mu_0(\boldsymbol{H}_d + \boldsymbol{M})$ yields

$$\nabla \cdot \boldsymbol{H}_d = -\nabla \cdot \boldsymbol{M} \quad . \tag{4.9}$$

The magnetostatic energy is the energy of the magnetization $\boldsymbol{M}$ in the field $\boldsymbol{H}_d$, therefore

$$E_{ms} = -\frac{1}{2}\mu_0 \int_V \boldsymbol{H}_d \cdot \boldsymbol{M} \, \mathrm{d}V \quad . \tag{4.10}$$

Here, one has to integrate over the volume V of the sample. The factor 1/2 takes into account the interaction of the magnetization with the field that is induced by itself (self-field energy).

With $\int \boldsymbol{B} \cdot \boldsymbol{H}_d \, \mathrm{d}V = 0$ (integration over the entire space)[5] and with $\boldsymbol{B} = \mu_0(\boldsymbol{H}_d + \boldsymbol{M})$ follows

$$E_{ms} = \frac{1}{2}\,\mu_0 \int \boldsymbol{H}_d^2 \, \mathrm{d}V \quad . \tag{4.11}$$

Both expressions, (4.10) and (4.11), can be used to calculate E_{ms}. The calculation of $\boldsymbol{H}_d$ can be very complex, and usually it is not possible to do this analytically. Simple relations apply in case of homogeneously magnetized ellipsoids with

$$\boldsymbol{H}_d = -\hat{N}\boldsymbol{M} \quad . \tag{4.12}$$

$\hat{N}$ is the demagnetization tensor, which is diagonal within the coordinate system of the principal axes of the ellipsoid

$$\hat{N} = \begin{pmatrix} N_x & 0 & 0 \\ 0 & N_y & 0 \\ 0 & 0 & N_z \end{pmatrix} \quad . \tag{4.13}$$

In special cases, $\hat{N}$ can be calculated analytically. For a thin film with normal vector in z-direction follows $N_x = N_y = 0$ and $N_z = 1$. For a sphere applies $N_x = N_y = N_z = 1/3$. An infinitely long cylinder along the z-direction yields $N_x = N_y = 1/2$ and $N_z = 0$.

The field $\boldsymbol{H}_d$ inside the sample is also denoted as demagnetization field, because it works against the magnetization. The part of $\boldsymbol{H}_d$ outside of the sample is the stray field. The absolute value of the demagnetization field $\boldsymbol{H}_d$ within the sample can maximally reach the M_s; this accounts also for the magnetization itself. With the normalization $\boldsymbol{m} \equiv \boldsymbol{M}/M_s$ and $\boldsymbol{h}_d \equiv \boldsymbol{H}_d/M_s$, Eq. (4.10) can be written as

$$E_{ms} = -\underbrace{\frac{\mu_0 M_s^2}{2}}_{\equiv K_d} \int_V \boldsymbol{h}_d \cdot \boldsymbol{m} \, \mathrm{d}V \quad . \tag{4.14}$$

[5] This follows under absence of currents from Amperes law $\nabla \times \boldsymbol{H} = \boldsymbol{j}$; see e.g. [Gross and Marx, 2012]; Ch. 12.1.4.

The prefactor $K_d \equiv \mu_0 M_s^2/2$ ('dipolar constant') therefore yields the order of magnitude of the magnetostatic self energy per volume. With $M_s \sim 10^6\,\mathrm{A/m}$, typical values for K_d are in the range $10^5 - 10^6\,\mathrm{J/m^3}$. From Eq. (4.14) follows the definition of the magnetostatic energy density $e_{ms} = -K_d \boldsymbol{h}_d \cdot \boldsymbol{m}$.

Except for the isotropic case of a spherical sample, for non-spherical sample geometries E_{ms} is anisotropic. In this case, this energy contribution is also termed 'shape anisotropy' E_{sh}. Different magnetic anisotropy energy contributions will be discussed in the following, where we also include the specific case of the shape anisotropy of thin films.

D. Magnetic anisotropy energy

The magnetization of a system usually points into a favoured direction (magnetic 'easy' axis); other directions ('hard' axes) are avoided. The (magnetic) anisotropy energy E_A describes the orientation-dependent contribution of the magnetization to the internal energy. If $\boldsymbol{M}$ points along an easy axis, then E_A is minimal; along a hard axis E_A is maximal.

The magnetic anisotropy is closely linked with the coercive field H_{coerc} of a ferromagnet; the quantitative relation of this link can be quite complex.The presence of anisotropy plays an important role for applications, e.g. in permanent magnets or in storage technologies.

In the most general case, the anisotropy energy density e_A (energy/volume) can be described by

$$e_A = K_A f(\theta, \varphi) \quad . \tag{4.15}$$

K_A is a general anisotropy parameter (which we shall specify below) in units of $\mathrm{J/m^3}$, and $f(\theta, \varphi)$ is a dimensionsless function of the angles describing the orientation of $\boldsymbol{M}$ in space.

We shall distinguish the following types of anisotropy energies, which may all enter into the total energy

- shape anisotropy (demagnetization energy) E_{sh}
- magnetocrystalline anisotropy E_{mc}
- surface anisotropy E_{su}

Other forms of anisotropy such as strain-induced or pressure-induced anisotropy may also enter. For instance, a uniaxial mechanical strain σ (due to epitaxial effects or externally applied stress) can induce a corresponding magnetic anisotropy via the magnetostriction parameter λ_s (e.g. -7×10^{-6} in Fe), leading to an energy density

$$e_{ind} = \frac{3}{2}\sigma\lambda_s \sin^2\Theta \quad , \tag{4.16}$$

with the angle Θ between $\boldsymbol{M}$ and the direction of strain. Generally, this leads to additional contributions to $f(\theta, \varphi)$ in Eq. (4.15), but are not conceptually different, so that, although important for a quantitative description of certain systems, we will not consider them further here.

(i) Shape anisotropy

The shape anisotropy E_{sh} is the magnetostatic energy associated with the surface and thus the shape of a sample, also known as demagnetization energy. Correspondingly, E_{sh} depends on the relative orientation between $\boldsymbol{M}$ and the principal axes of the sample shape. It is only negligible for spherical samples. For thin films, e.g., it is a very significant contribution, trying to force $\boldsymbol{M}$ into the plane of the film.

The shape anisotropy is closely linked to the magnetostatic energy, as already mentioned above: it is based on the anisotropy of the demagnetization tensor $\hat{N}$. The shape anisotropy is the amount of energy that is required to rotate the magnetization away from the energetically most favourable direction. For a sphere, E_{sh} is obviously zero, because for each direction $N = 1/3$. For a thin film with normal vector $\hat{\boldsymbol{n}}$ and angle Θ between $\hat{n}$ and M, e_{sh} is given by [6]

$$e_{sh} = -\frac{\mu_0}{2} M_s^2 \sin^2\Theta = -K_d \sin^2\Theta \quad . \tag{4.17}$$

(ii) Magnetocrystalline anisotropy

The magnetocrystalline anisotropy (described by the energy density e_{mc}) causes the preferred alignment of the magnetization along a certain cristallographic direction. The reason for this is the spin-orbit coupling, i.e., the connection of the electron spins with the orbital moments of the electrons. For elements, whose shells are not completely filled (e.g. $3d$-electrons in transition metals or $4f$-electrons in rare earth elements), the electron distribution is no longer spherical (see Fig. 4.4). A rotation of the magnetization, thus a rotation of the spins, causes a rotation of the electron orbital distribution. This changes the overlap of the wave functions and hence the exchange energy and electrostatic interaction energy. The angular dependence $e_A(\theta, \varphi)$ of the magnetocrystalline anisotropy e_{mc} of course has to be consistent with the underlying symmetry of the crystal, i.e., for a cubic crystal the six [100] directions have to be energetically equivalent (hard or easy axes depending on the sign of the parameter K_{mc}).

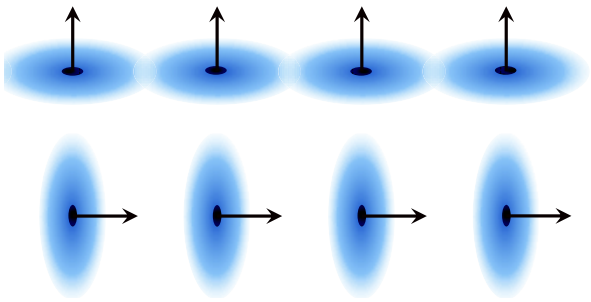

Fig. 4.4: On the origin of the magnetocrystalline anisotropy: A non-spherical charge distribution is coupled to the spin direction via the spin-orbit-coupling; different magnetization directions (spin directions) therefore lead to a different exchange interaction and electrostatical interaction. From [Gross and Marx, 2012].

The simplest case is for uniaxial anisotropy, which can be expanded in the form

$$e_{mc} = K_1 \sin^2\Theta + K_2 \sin^4\Theta \quad + ..., \tag{4.18}$$

where Θ is the angle of $\boldsymbol{M}$ with the easy axis. Frequently, the $\sin^4$ term can already be neglected. Equation (4.18) is typical for hexagonal crystals.

[6] $\boldsymbol{H}_D = -\hat{\boldsymbol{n}}\boldsymbol{M} \rightarrow \boldsymbol{h}_D = -\cos\theta\hat{\boldsymbol{n}} \Rightarrow e_{ms} = -K_D \boldsymbol{h}_d \boldsymbol{m} = K_D \cos\theta\hat{\boldsymbol{n}}\boldsymbol{m} = K_D \cos^2\theta = K_D - K_D \sin^2\theta$. For e_{sh} one omits the term K_D, as this does not depend on θ.

(iii) Surface anisotropy

As first pointed out by L. Néel [Néel, 1953, Néel, 1954] the presence of a surface (and thus the different environment of the surface atoms with their reduced number of neighbors) inevitably leads to a magnetic surface anisotropy with energy density

$$e_{su} = K_{su} \sin^2 \Theta \tag{4.19}$$

which is an energy per area. Here, Θ is the angle of M relative to the surface normal. Its contribution to the total energy of the system is obtained accordingly by integrating over the sample *area*. Note that, depending on the specific material, K_{su} can have either sign; in most cases, $K_{su} > 0$ which favours an out-of-plane magnetization.

The angular dependence of e_{su} is in many cases the same as that of the shape anisotropy and potentially other contributions, which enter as volume densities, in contrast to e_{su}, which is a surface density. The interplay or competition of the different contributions is best illustrated for the case of a thin film with shape anisotropy as in Eq. (4.17), with (volume) energy density $e_{sh} = -K_d \sin^2 \Theta$ and $e_{su} = K_{su} \sin^2 \Theta$.

For the comparison of the two terms we either integrate e_{sh} over the volume (area times film thickness d_f) and e_{su} over the surface area, or consider the volume densities in both cases after dividing e_{su} by d_f. The latter leads to an effective anisotropy (volume) energy density of the type (neglecting magnetocrystalline contributions)

$$e_A = -K_d \sin^2 \Theta + \frac{2K_{su}}{d_f} \sin^2 \Theta = -\underbrace{\left(K_d - \frac{2K_{su}}{d_f} \right)}_{K_{eff}} \sin^2 \Theta \tag{4.20}$$

where the factor of 2 in front of K_{su} takes into account the two surfaces (top and bottom) of the thin film. Here K_{eff} is an effective anisotropy parameter. For $K_{eff} > 0$, the shape anisotropy term $K_d = \frac{\mu_0}{2} M_s^2$ dominates over the surface anisotropy term, and hence, the alingment of the magnetization in the thin film plane is energetically favorable. For $K_{eff} < 0$, the surface anisotropy dominates, and the out-of-plane magnetization is preferred.

The interplay between shape and surface anisotropy in thin films can be studied in experiments, where an effective magnetization M_{eff} can be measured, defined as [7]

$$M_{eff} \equiv M_s \frac{K_{eff}}{K_d} = M_s - \frac{4K_{su}}{\mu_0 M_s} \frac{1}{d_f} \tag{4.21}$$

For pure shape anisotropy $M_{eff} = M_s$, i.e., the applied field is modified by the demagnetization field given by M_s which points along the surface normal. This is reduced with decreasing d_f due to the contribution of the surface anisotropy term. The resulting effective magnetization M_{eff} is shown in Fig. 4.5 plotted vs. $1/d_f$. Then the limit of $1/d_f \to 0$ is given by the volume term M_s, and the slope is given by K_{su}, which can, in principle, have either sign. For $K_{su} > 0$ the total function cuts the zero-line for sufficiently thin $d_f = d_c = 2K_{su}/K_d$. For $d_f < d_c$ the shape anisotropy is thus overcome and the magnetization points preferentially *along* the surface normal. Typical parameters are $K_{su} \sim 10^{-3}\,\mathrm{J/m^2}$, and $K_d \sim 10^6\,\mathrm{J/m^3}$ implying that $d_c \sim 20\,\mathring{A}$. This

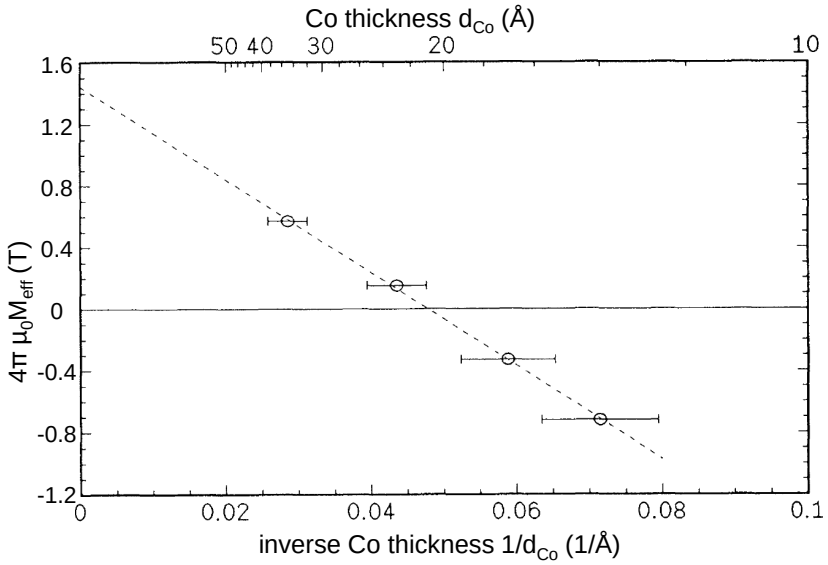

Fig. 4.5: Effective magnetization M_{eff} as a function of inverse Co thickness for Co/Cr(001) superlattices measured by ferromagnetic resonance (FMR) and MOKE. The broken line is a fit to the data. Adapted from [Schreiber et al., 1995].

effect of *perpendicular magnetization* as the ground state for zero external field is very important for magnetic recording technology and is caused by K_{su}.

D. Total energy and characteristic quantities

The total energy of a magnetic system with imhomogeneous magnetization can be calculated within the micromagnetic model (assumption: locally saturated areas within the volume element $\mathrm{d}V$) by integration over the various contributions to the energy density (e_{ex}, e_A, e_{ms}, e_Z):

$$E_{tot} = \int_V \left\{ \underbrace{\frac{A}{M_s^2}(\nabla \boldsymbol{M})^2}_{exchange} + \underbrace{K_A e_A(\theta,\varphi)}_{anisotropy} - \underbrace{\frac{\mu_0}{2}\boldsymbol{M}\cdot\boldsymbol{H}_d}_{magn.static} - \underbrace{\mu_0 \boldsymbol{M}\cdot\boldsymbol{H}_{ext}}_{Zeeman} \right\} \mathrm{d}V \quad . \tag{4.22}$$

For the case of an uniaxial anisotropy of the general form $e_A = K_1 e_A(\Theta)$, with the normalization $\boldsymbol{m} \equiv \boldsymbol{M}/M_s$, $\boldsymbol{h}_d \equiv \boldsymbol{H}_d/M_s$ and $\boldsymbol{h}_{ext} \equiv \boldsymbol{H}_{ext}/M_s$, and from the definition of K_d in (4.14) follows

$$E_{tot} = K_d \int_V \left\{ \underbrace{\frac{A}{K_d}}_{\equiv l_{ex}^2} (\nabla \boldsymbol{m})^2 + \underbrace{\frac{K_1}{K_d}}_{\equiv \kappa} e_A(\Theta) - \boldsymbol{m}\cdot\boldsymbol{h}_d - 2\boldsymbol{m}\cdot\boldsymbol{h}_{ext} \right\} \mathrm{d}V \quad . \tag{4.23}$$

The prefactor A/K_d in the first term (exchange energy) of the integral can be identified with the square of a characteristic length l_{ex}. This so-called *exchange length* is given as

$$l_{ex} \equiv \sqrt{\frac{A}{K_d}} = \sqrt{\frac{2A}{\mu_0 M_s^2}} \quad . \tag{4.24}$$

[7] In the literature such relations are often given in cgs units; in this case Eq.(4.21) transforms into $4\pi M_{eff} = 4\pi M_s - 4K_s/(M_s d_f)$

For lengths smaller than l_{ex}, the exchange energy dominates over the magnetostatic energy. This means that if one changes the magnetization on a length scale $< l_{ex}$, then the exchange term becomes very large as compared to the magnetostatic energy. Typical values of l_{ex} are in the range of a few nanometers.

The prefactor in the second term (uniaxial anisotropy energy) in the integral (4.23) is the so called 'hardness parameter'

$$\kappa \equiv \frac{K_1}{K_d} = \frac{2K_1}{\mu_0 M_s^2} \quad . \tag{4.25}$$

It quantifies the ratio of the contribution of the anisotropy energy over the magnetostatic self energy ($\sim 0.03 - 0.3$ in 3d-metals)

The ratio of l_{ex} and $\sqrt{\kappa}$ defines another characteristic length, the so-called anisotropy exchange length (or Bloch-parameter):

$$\Delta = \frac{l_{ex}}{\sqrt{\kappa}} = \sqrt{\frac{A}{K_1}} \quad . \tag{4.26}$$

This quantity determines the thickness of a domain wall (several 10 – 100 nm). A simple estimate yields the domain wall thickness (see below)

$$\delta_0 = \pi\sqrt{2} \cdot \Delta = \pi\sqrt{2}\sqrt{\frac{A}{K_1}} \quad . \tag{4.27}$$

And finally, the product $l_{ex}\sqrt{\kappa} = \sqrt{AK_1}/K_d$ provides us with another characteristic length, the so called critical domain diameter (see below)

$$D_{cr} = 36 l_{ex}\sqrt{\kappa} = \frac{72\sqrt{AK_1}}{\mu_0 M_s^2} \quad , \tag{4.28}$$

which can vary from several nm up to a μm.

4.3.2 Magnetic Domains

The magnetostatic energy of a single-domain system increases with its volume. Above a critical diameter D_{cr}, it is therefore energetically favourable to form domains of different magnetization directions. In the simplest case of an uniaxial anisotropy, the magnetization of both domains is aligend along the easy axis in an antiparallel configuration. The direction of the magnetization therefore changes across the interface between the two domains, leading to the formation of a domain wall. Since the moments are no longer parallelly aligned within a domain wall and deviate from the easy axis direction, the formation of a domain wall increases the exchange energy and the anisotropy energy.

There are two types of domain walls: the Bloch wall and the Néel wall (see Fig. 4.6). In the Bloch wall, the magnetization rotates within the wall plane. If the sample size is significantly larger than the wall thickness, there is no magnetostatic contribution to the wall energy. However, in the case of thin films with the easy axis lying in the film plane, the Bloch wall induces a large additional contribution to the magnetostatic energy; this is because the rotating moments are pointing out of the film plane. In that case, the formation of a Néel wall is more favourable. In a Néel wall, the magnetization rotates within the film plane, perpendicular to the domain wall.

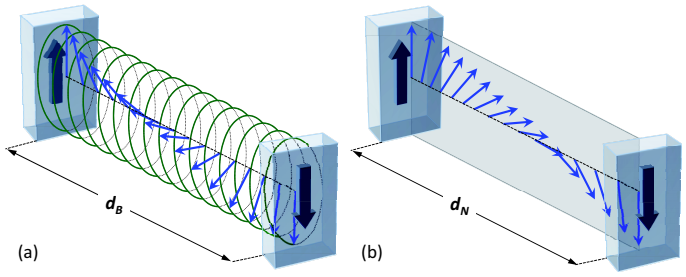

Fig. 4.6: Schematic representation of the spin orientation of a 180° **Bloch wall (a)** and a 180° **Néel wall (b)** between two antiparallelly oriented magnetic domains. From [Gross and Marx, 2012].

Domain wall thickness

We consider a Bloch wall in a system with uniaxial anisotropy, with a rotation of the magnetization by 180° (see Fig. 4.6(a)). The smaller the angle between adjacent moments, the lower is the contribution of the domain wall to the exchange energy. Hence, it is energetically favourable to distribute the 180° Bloch wall over as much spins as possible along the wall, i.e., to maximize the wall thickness. However, the thicker the wall, the more spins deviate from the easy axis direction, and the larger is the contribution to the anisotropy energy of the wall. Therefore, magnetic anisotropy favours a wall that is as thin as possible.

As a result of the above mentioned competition, the wall thickness δ_0 depends on the ratio of exchange energy and anisotropy energy. We can estimate both contributions by considering a wall which consists of N lattice planes with lattice spacing a. If we assume a constant rotation angle $\Delta\Theta = \pi/N$ of the magnetization between adjacent lattice planes, this yields the energies per wall area $\epsilon_{ex} = \pi^2 A/aN$(sheet density of exchange energy) and $\epsilon_A = K_1 Na/2$ (sheet density of anisotropy energy) [Guimarães, 2009]. The minimization of $\epsilon_{dw}(N) = \epsilon_{ex}(N) + \epsilon_A(N)$ with respect to N yields the domain wall thickness

$$\delta_0 = Na = \pi\sqrt{2}\sqrt{\frac{A}{K_1}} \quad . \tag{4.29}$$

As expected, the Bloch wall thickness is determined by the ratio A/K_1 This results in an energy density of the wall

$$\epsilon_{dw} = \pi\sqrt{2}\sqrt{AK_1} \quad , \tag{4.30}$$

which contains equal contributions from ϵ_{ex} and ϵ_A.

The exact calculation [Fruchart, 2015] yields the spatial dependence of the angle

$$\Theta(x) = 2\arctan\{e^{x/\Delta}\} \quad \text{with} \quad \Delta \equiv \sqrt{\frac{A}{K_1}} \tag{4.31}$$

along the coordinate x, perpendicular to the domain wall (centered at $x = 0$), with a slightly lower density of the wall energy $\epsilon_{dw} = 4\sqrt{AK_1}$.

In case of Néel walls, $-\nabla \cdot \boldsymbol{M}$ does not vanish (in contrast to Bloch walls). Hence,one has to take into account that magnetostatic contribution if one wants to calculate the wall thickness δ_0 and the energy density e_{dw} of the wall. The calculation yields comparable expressions, however, K_1 has to be replaced by $K_1 + K_d$.

Critical single-domain size

For a ferromagnetic system it is energetically favourable to build two (or more) domains with different directions of magnetization instead of a homogeneous magnetiziation (single-domain-state), if the system sized exceeds the critical domain diameter.

To estimate the maximum domain size, we compare the single-domain state with the two-domain state for the simple case of an ellipsoidal particle (see Fig. 4.7) and search for the critical domain diameter for which both configurations have the same energy.

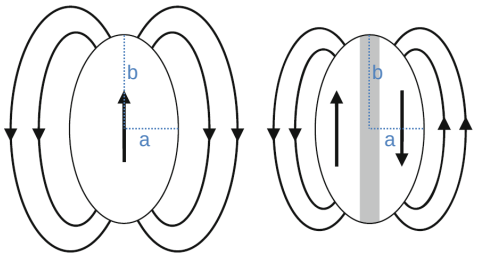

Fig. 4.7: Magnetic particle (ellipsoid with semiaxes a and b) in single-domain (left), and two-domain state (right). Magnetization direction inside the particle, stray-field configuration and domain wall (grey) are indicated. From [Guimarães, 2009].

The following considerations apply to the case of $H_{ext} = 0$ and an axially symmetric ellipsoid with semiaxes of lengths a and b; the latter shall be the easy axis of for uniaxial anisotropy. The magnetization, which is homogeneous within the domain(s), is aligned along the easy axis, such that in Eq. (4.22) not only the Zeeman term, but also the anisotropy term and the exchange term are zero (except for the contribution from the domain wall). Therefore the only contributions are the magnetostatic energy E_{ms} and the domain wall energy E_{dw}.

single-domain configuration:
With the particle volume $V = \frac{4}{3}\pi a^2 b$, and the demagnetization factor $N_{||}$ along the long principal axis ($b > a$), the energy can be written as

$$E(1) = E_{ms}(1) = -\frac{1}{2}\mu_0 \boldsymbol{H}_d \boldsymbol{M} \cdot V = N_{||} K_d \cdot \frac{4}{3}\pi a^2 b \quad . \tag{4.32}$$

two-domain configuration:
Using an Ansatz for the stray field energy that is reduced by the factor $\alpha < 1$, and with the additional domain wall energy (with energy per area ϵ_{dw} and domain wall area πab) one obtains

$$E(2) = E_{ms}(2) + E_{dw} = \alpha N_{||} K_d \cdot \frac{4}{3}\pi a^2 b + \pi ab\, \epsilon_{dw} \quad . \tag{4.33}$$

Then, from $E(1) = E(2)$ follows for the critical diameter

$$D_{cr} = 2a = \frac{3}{2N_{||}(1-\alpha)} \cdot \frac{\epsilon_{dw}}{K_d} \quad , \tag{4.34}$$

which scales with a geometry-dependent constant and with the ratio of wall energy over magnetostatic energy.

With $\epsilon_{dw} = 4\sqrt{AK_1}$, one obtains for a sphere ($a = b$) with $N_{||} = 1/3$ and [8] $\alpha \approx 1/2$

$$D_{cr} = 36\frac{\sqrt{AK_1}}{K_d} = 72\frac{\sqrt{AK_1}}{\mu_0 M_s^2} \quad . \tag{4.35}$$

For a fixed saturation magnetization M_s ($K_d = const$), D_{cr} increases linearly with the domain wall energy. The more energy the formation of a domain wall costs, the larger can be the particle in the single-domain state. Figure 4.8 shows the scaling of D_{cr} with the anisotropy parameter of different magnetic materials.

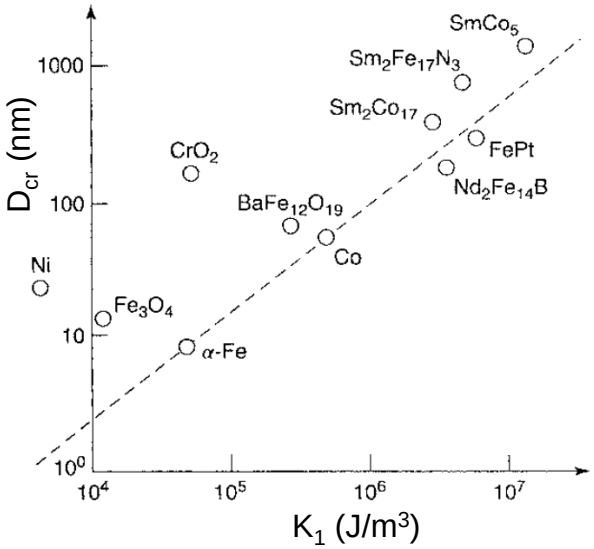

Fig. 4.8: Critical domain diameter vs. anisotropy parameter for different magnetic materials. From [Guimarães, 2009].

[8] More accurate calculations yield $\alpha = 0.472$ for a sphere.

Finally, Tab. 4.2 shows values of some of the parameters which have been introduced in this chapter for various ferromagnetic materials.

Table 4.2: Micromagnetic parameters of some materials at room temperature: saturation magnetization M_s, dipolar constant $K_d = \mu_0 M_s^2/2$, exchange stiffness constant A, exchange length l_{ex}, domain wall width δ_0, critical single-domain diameter D_{cr} (with $\alpha = 0.472$) and domain wall energy density ϵ_{dw}. From [Guimarães, 2009].

Material	M_s (RT) (10^6A/m)	K_d (10^6J/m^3)	A (10^{-12}J/m)	l_{ex} (nm)	δ_0 (nm)	D_{cr} (nm)	ϵ_{dw} (10^{-3}J/m^2)
Fe	1.714	1.84	19.8	3.28	63.7	19	3.9
Co	1.422	1.27	28.1	4.70	25.9	96	14
Ni	0.484	0.15	8.6	7.64	123	54	0.88
$Ni_{0.8}Fe_{0.2}$	0.813	0.42	10.7	5.08	625	4.7	0.22
$Nd_2Fe_{14}B$		1.03		2.8	3.82	210	24
$SmCo_5$		0.44		5.3	2.64	1170	57
Sm_2Co_{17}				4.6	5.74	420	31
$BaFe_{12}O_{19}$		0.09		8.3	1.94	62	6.3

4.4 Magnetic Nanoparticles (MNPs)

We consider now the magnetic properties of systems which do have small size on the nanometer scale in all three dimensions, i.e. magnetic nanoparticles (MNPs), including single molecule magnets (SMMs).

4.4.1 MNP Basics

Going from macroscopic magnetically ordered systems to nanoscale MNPs, their properties can change drastically. To illustrate this, Fig. 4.9 shows a schematic view of the scaling of the size of magnetic systems from macroscopic to nanoscopic with the number of spins going down from $S = 10^{20}$ to $S = 1$.

The $M(H)$ hysteresis loops reveal a drastic change in the nature of the magnetization reversal process, going from domain wall nucleation and propagation in the multi-domain state for large systems, through the uniform rotation of magnetization in the single-domain state to quantum tunneling of magnetization at low temperature.

To provide an understanding of this behavior is a severe challenge in the field of MNPs, which is currently a very active research field.

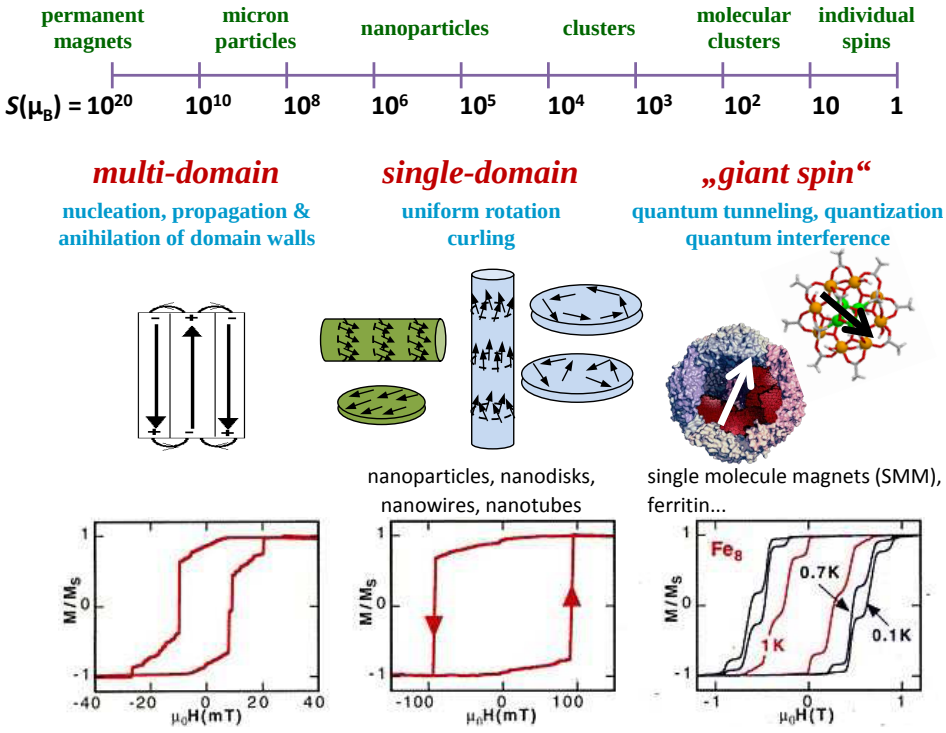

Fig. 4.9: Scaling from macroscopic down to nanoscopic magnetic systems. S is the number of magnetic moments in μ_B (roughly corresponding to the number of atoms). The hysteresis loops $M(H)$ show typical measurements of magnetization reversal. Adapted from [Wernsdorfer, 2001].

Problem for characterization

Very small volume gives rise to very small signals, e.g. in susceptibility (magnetization) measurements → very hard to investigate properties of *single* MNPs or SMMs.

→ most measurements are made on large ensembles of MNPs

Disadvantages of measurements on ensembles:

- includes interactions between MNPs
- no information on magnetic anisotropy of single MNPs (for randomly oriented ensembles)
- strong dependence of magnetic properties on MNP size and shape
  → only information on averaged properties

⇒ measurements on ensembles give only very limited information on properties of *single* MNPs

→ hard to synthesize MNPs with well defined size and shape
→ typically, ensembles of MNPs are non-uniform (polydisperse)

Here, SMMs are of significant advantage, since they can be synthesized in large quantities of identical units → monodisperse ensembles.

Characterization methods on single MNPs

During the last two decades a variety of extremely sensitive techniques has been developed. Those are able to perform spectroscopy and/or magnetometry on single MNPs, approaching sensitivities on the level of a single electron spin (one Bohr magneton).

- spin-polarized scanning tunneling microscopy/spectroscopy [Bode et al., 2004].
- photo-emission electron microscopy (PEEM) combined with X-ray magnetic circular dichroism (XMCD) [Kleibert and Nolting, 2013].
- magnetic resonance force microscopy (MRFM) [Poggio and Degen, 2010, Rugar et al., 2004].
- nanoscale magnetometry with nitrogen-vacancy centers in diamond [Degen, 2008].
- torque magnetometry/microscopy [Buchter et al., 2013].
- nanoSQUID magnetometry/microscopy
  [Wernsdorfer, 2009, Martínez-Pérez and Koelle, 2017].

Single-Domain Particles

In macroscopic ferromagnetic samples, the minimization of the total energy favors the formation of a multi-domain state. The reversal of the overall magnetization of the sample upon applying a magnetic field $\boldsymbol{H}$ typically occurs via the formation and motion

of magnetic domain walls. With decreasing sample size, the coercive field $\boldsymbol{H}_{\text{coerc}}$ tends to increase (Fig. 4.10). This is because the magnetostatic self energy (which favors domain formation) is significantly reduced, and magnetization reversal via domain wall nucleation and motion is impeded.

For MNPs with diameter D below the critical single-domain diameter D_{cr}, the formation of domain walls becomes energetically unfavorable → such particles are in a single-domain state, even at $\boldsymbol{H} = 0$. Magnetization reversal of single-domain particles then has to occur via coherent rotation of their spins upon applying $\boldsymbol{H}$. In this case, $\boldsymbol{H}_{coerc}$ is basically determined by the anisotropy energy, but also depends, e.g. , on the orientation of the external field, relative to the easy axis.

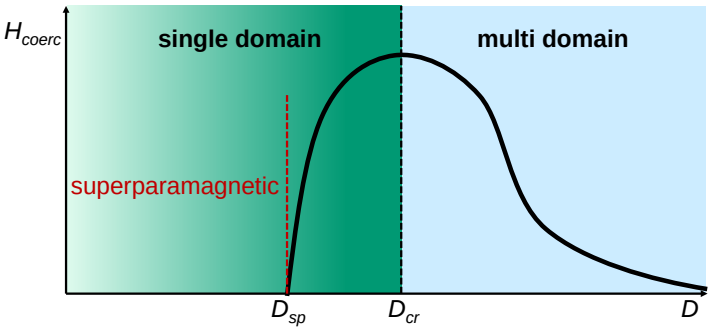

Fig. 4.10: Qualitative illustration of the behavior of the coercive field H_{coerc} in MNPs as the particle size D changes. Adapted from [Hornyak et al., 2009].

As the particle size continues to decrease, the switching of $\boldsymbol{M}$ induced by thermal fluctuations becomes increasingly important, yielding a decreasing H_{coerc} with decreasing D until the superparamagnetic limit at diameter D_{sp} is reached, where $H_{\text{coerc}} = 0$ (Fig. 4.10). Figure 4.11 shows for some selected materials typical values for D_{cr} and D_{sp} at room temperature.

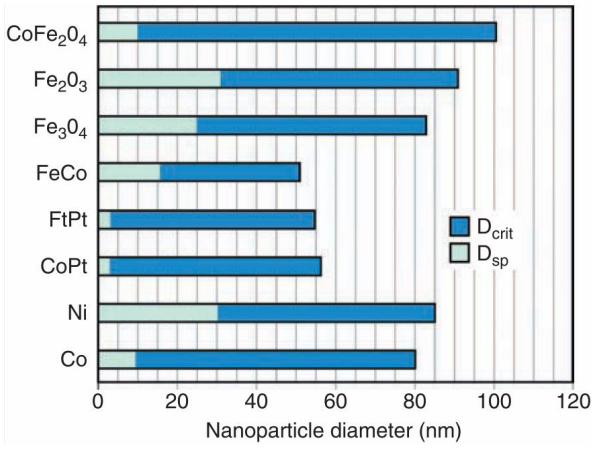

Fig. 4.11: Critical single-domain diameter D_{cr} and superparamagnetic critical diamter at room temperature, D_{sp} for some common ferromagnetic materials. From [Hornyak et al., 2009].

At low enough temperatures and small enough energy barriers (anisotropy energy), coherent tunneling between different magnetization states can become the dominant process of magnetization reversal [Wernsdorfer, 2001, Bartolomé et al., 2014].

The Stoner-Wohlfarth model

The model of uniform reversal of magnetization $\boldsymbol{M}$ was developed by Stoner and Wohlfarth [Stoner and Wohlfarth, 1948] and by Néel [Néel, 1947] in the late 1940s, as the simplest classical model describing magnetization reversal.

This model assumes ideal homogeneous alignment of all spins, such that $|\boldsymbol{M}| = const. = M_s$, i.e. the magnitude of the magnetization does not depend on space and orientation and is given by the saturation magnetization M_s. In this case, the exchange energy is constant → does not play a role in energy minimization. For spherical particles, also the magnetostatic energy does not depend on the orientation of $\boldsymbol{M}$ → does also not play a role in energy minimization.

For anisotropic systems, there is a competition between the anisotropy energy and the effect of an applied magnetic field $\boldsymbol{H}$ (Zeeman energy).[9]

In the simplest case of uniaxial anisotropy, the energy of a particle is given by

$$E = K_1 V \sin^2(\theta) - \mu_0 H M_s V \cos(\theta - \phi) \quad , \tag{4.36}$$

with the particle volume V and uniaxial anisotropy parameter K_1. Here, θ is the angle of M, and ϕ is the angle of H – both with respect to the easy axis of magnetization (see Fig. 4.12).

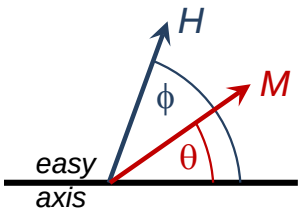

Fig. 4.12: Definition of angles between $\boldsymbol{M}$, $\boldsymbol{H}$ and the easy axis.

For simplicity, we now assume $\phi = \pi$, i.e., H opposite to initial direction ($\theta = 0$) of M along the easy axis. Introducing the *anisotropy field* $H_a \equiv 2K_1/(\mu_0 M_s)$ and the normalization $\epsilon \equiv E/K_1 V$ and $h \equiv H/H_a$, Eq. (4.36) reads

$$\epsilon = \sin^2(\theta) + 2h\cos(\theta) \quad . \tag{4.37}$$

Figure 4.13 shows $\epsilon(\theta)$ for various values of the normalized magnetic field h. Due to the symmetry of the problem, it is sufficient to consider values for θ in the interval $[0, \pi]$. For the sake of clarity, we show $\epsilon(\theta)$ for the interval $-\pi \leq \theta \leq \pi$, although the angle θ is equivalent to $-\theta$, i.e. $\epsilon(\theta) = \epsilon(-\theta)$.

Starting at $h = 0$, the potential energy $\epsilon(\theta)$ of (4.37) has two minima at $\theta = 0$ and π, separated by an energy barrier, the height of which is $\Delta\epsilon = 1$ (i.e. $\Delta E = K_1 V$). With increasing h, the minimum at $\theta = 0$ is lifted up and disappears at $h = 1$. This means, H_a is the threshold field required to overcome the energy barrier to switch the magnetization to the $\theta = \pi$ state. For $\phi = \pi$ switching of magnetization occurs abruptly at the switching field $H_{sw} = H_a$ from $\theta = 0$ to $\theta = \pi$, i.e. the $M(H)$ curve is rectangular shaped.

[9] Stoner and Wohlfarth originally only assumed uniaxial shape anisotropy, i.e. the anisotropy of the magnetostatic energy of a non-spherical sample. This was generalized later to an arbitrary effective anisotropy, including any magnetocrystalline anisotropy and surface anisotropy.

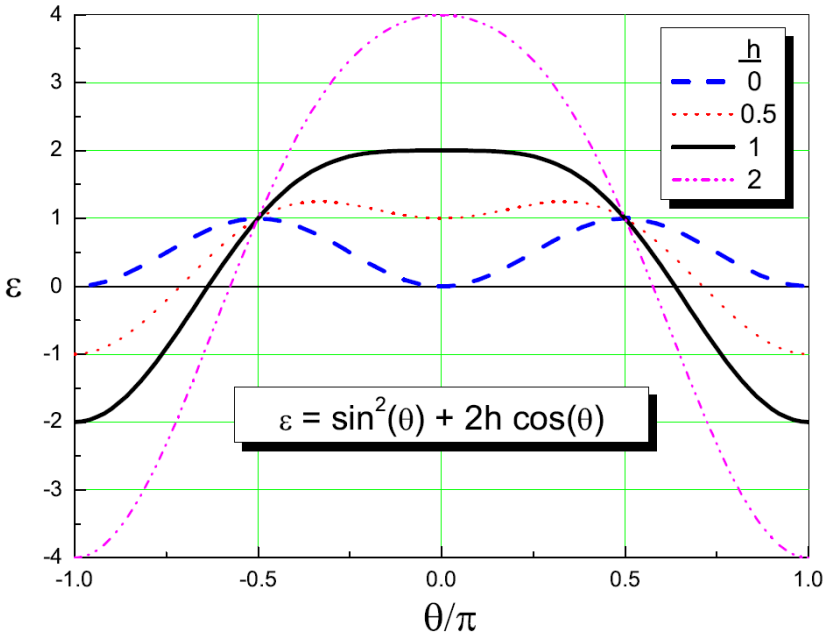

Fig. 4.13: Normalized energy $\epsilon = E/K_1V$ of a monodomain MNP vs angle θ of magnetization (with respect to easy axis for uniaxial anisotropy) for different values of normalized external magnetic field $h = H/H_a$ at angle $\phi = \pi$ with respect to the easy axis, calculated within the Stoner-Wohlfarth model from Eq. (4.37).

For increasing deviation of the angle of applied field from $\phi = \pi$ (or 0), the Stoner-Wohlfarth model predicts an increasing rounding of the $M(H)$ curves and a reduction of the switching field H_{sw}. Calculations for different values for ϕ are shown in Fig. 4.14.

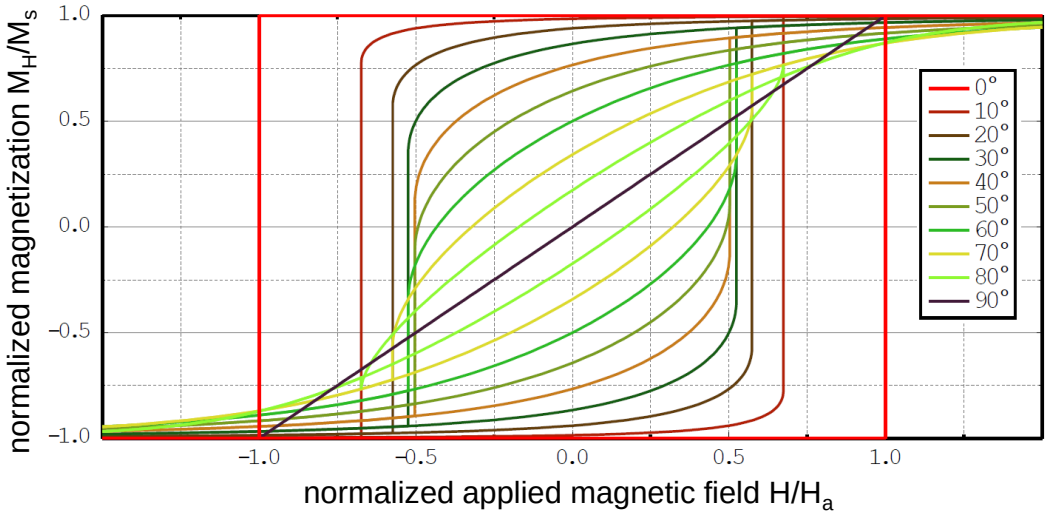

Fig. 4.14: $M(H)$ hysteresis loops calculated with Stoner-Wohlfarth model for different angles ϕ of the applied field H, normalized to H_a. The vertical axis is the component M_H of $\boldsymbol{M}$ along the direction of H, normalized to M_s. From [Fruchart, 2015].

Superparamagnetic Limit

We consider a MNP in the single-domain state at $H = 0$. The orientation of $\boldsymbol{M}$ will be along the magnetically easy axis, and there exist two possible magnetization directions (differing by 180 °), which are energetically equivalent. Those two states are separated by an energy barrier $K_1 V$, given by the anisotropy energy density K_1 times sample volume V.

The reversal of $\boldsymbol{M}$ can be induced by thermal activation over this energy barrier. In this case, the relaxation time can be described by a simple Arrhenius law as

$$\tau = \tau_0 \exp\left(\frac{K_1 V}{k_B T}\right) \quad , \tag{4.38}$$

with a characteristic time τ_0.

If we take as representative values $\tau_0 = 1\,\text{ns}$, $K_1 = 0.1\,\text{J/cm}^3$, $T = 300\,\text{K}$ and a particle diameter $D = 11.4\,\text{nm}$, one finds a relaxation time $\tau \approx 0.14\,\text{s}$. If we increase the particle diameter slightly to $D = 14.6\,\text{nm}$, the relaxation time will increase to $\tau \approx 2 \times 10^7\,\text{s}$ $\approx 8\,\text{months}$!!

If we perform a measurement of any magnetic property (e.g. susceptibility) within the measurement time τ_i given by the measuring instrument, we can define a *blocking temperature*

$$T_B = \frac{K_1 V}{k_B \ln(\tau_i/\tau_0)} \quad , \tag{4.39}$$

i.e., T_B is the temperature which induces relaxation by thermal activation at the relaxation time $\tau = \tau_i$. This means, that at temperatures $T < T_B$, the relaxation time $\tau > \tau_i$, and our measurement can detect the ferromagnetic nature of the sample (e.g. hysteresis loop). On the other hand, for temperatures $T > T_B$, the relaxation time $\tau < \tau_i$; i.e. on the (larger) time scale of our measurement, we will see a vanishing (time averaged) magnetization. In this case the system is in an apparent paramagnetic state, even though at any time the sample has all spins ferromagnetically aligned – this is called the *superparamagnetic state*.

Ferrofluids

In a ferrofluid, sufficiently small MNPs are brought into a colloidal suspension, which contains three ingredients:

- liquid carrier (water- or oil-based)
- ferromagnetic particles (diameter $D \sim 10 - 20\,\text{nm}$): magnetite, cobalt, cobalt-ferrite → particle size has to be small enough to avoid precipitation
- surfactant coating of MNPs: reduces surface tension to support stability of colloidal suspension (alternatively, charged particles are used)

⇒ synthetic liquids with magnetic susceptibility $\chi \sim 1 - 10$
($\chi \approx 10^{-3}$ for liquid oxygen as the strongest natural paramagnetic liquid)

The magnetic properties of ferrofluids strongly depend on particle size and concentration. An applied magnetic field is used to magnetize the fluid. The agglomeration

of the MNPs due to magnetic interactions are opposed by the thermal energy of the particles. The MNPs can move freely under the influence of an external magnetic field, but on average their spacing s stays almost constant. For low-density fluids (few volume percent MNPs): $s \gg D$, i.e. dipole-dipole interactions are very small. Applied magnetic field gradients induce a force on the fluid (towards the direction of increasing field). The large susceptibility allows to maintain stable deformation of the liquid against the gravitational force.

Basic physical phenomenon – Rosensweig instability [Richter, 2008]

Consider a ferrofluid in a homogeneous external field H applied perpendicular to the fluid surface → no net force on the fluid.

Small disturbances can induce deviations from a flat surface
→ regions of thicker (thinner) liquid → local flux density B increases (decreases)
⇒ induces inhomogeneous flux density distribution.

For B larger than a critical flux density B_{crit}:
The self-induced flux density maxima are strong enough to attract more fluid
→ growth of "liquid mountains" against gravitation and surface tension,
which further increase the local flux gradients (Fig. 4.15).
The flat fluid surface becomes unstable → Rosensweig instability [Cowley and Rosensweig, 1967].

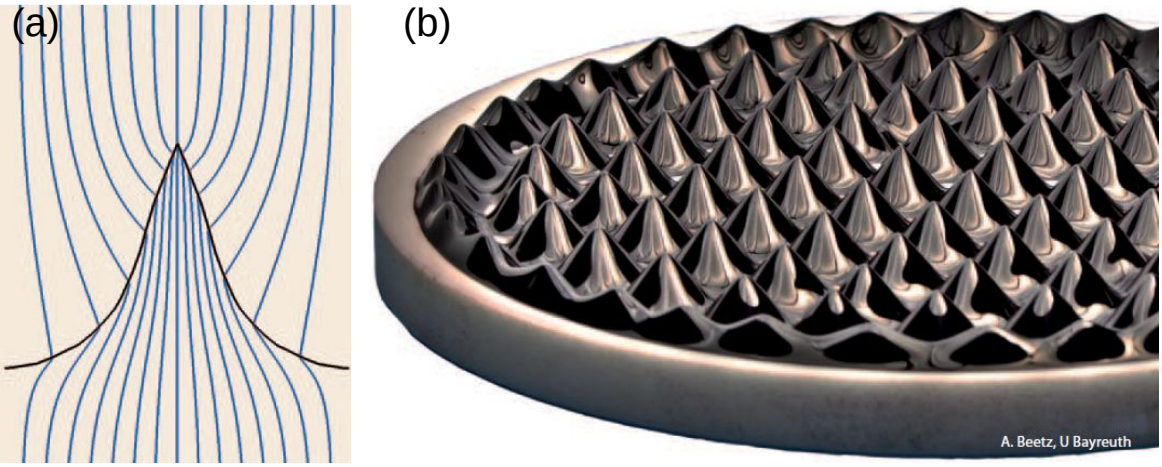

Fig. 4.15: Rosensweig instability in a ferrofluid: (a) Magnetic field lines concentrate at the tip of a ferrofluid ($\chi \sim 10$); (b) Photograph of a ferrofluid subjected to a homogeneous perpendicular magnetic field. From [Richter, 2008].

An analysis of the competing energies (hydrostatic, surface and magnetic field energies) yields

$$B_{\text{crit}} = \frac{\sqrt{2\mu_0(\chi+1)(\chi+2)\sqrt{\rho g \sigma}}}{\chi} \quad , \tag{4.40}$$

with the ferrofluid density ρ, gravitational acceleration g and surface tension σ.

With $\chi = 1$, $\rho = 1\,\text{g/cm}^3$ and $\sigma = 2 \times 10^{-2}\,\text{N/m}$, one obtains $B_{\text{crit}} \approx 15\,\text{mT}$ from Eq. (4.40), which is easily accessible experimentally.

Most often, the generation of spatio-temporal patterns in nature is a phenomenon which is observed in systems driven far from thermodynamic equilibrium. In that sense, the Rosensweig instability is a quite unusual phenomenon, as it is observed in a system at thermal equilibrium (no energy dissipation). Hence, from a basic view of physics, this is an interesting system in the field of non-linear dynamics, as it is complementary to most other systems in which pattern generation is observed.

Applications of ferrofluids

Applications are based on the possibility to control the shape and position of the fluid by an applied magnetic field or field gradient. Some examples are

- Rotary shaft seals (e.g. in hard disc drives)
- Magnetic liquid seals
- Cooling and resonance damping for loudspeaker coils
- Printing with magnetic ink
- Fluid level sensors
- Electromagnetically triggered drug delivery

4.4.2 MNP Applications

Most widely studied fields of applications for MNPs (often Fe_xO_y particles) are

- ferrofluids
- high-density information storage
- magnetic resonance imaging (MRI)
- biological cell labeling, sorting and separation of biochemicals
- targeting, and drug delivery

Depending on the specific applications, the surface of the MNPs is modified/coated by physical or chemical adsorption [Lu and an F. Schüth, 2007]. For example, Fe_xO_y MNPs are coated by silica (SiO_2) to prevent their aggregation in liquids and to improve their chemical stability.

Another example is the grafting of MNPs with a polymer [e.g. poly(1-vinylimidazole)] for applications as magnetic carriers. Such an organic-inorganic hybrid system can be used in applications ranging from biological cell sorting to industrial effluent detoxification and recovery of valuables (e.g. removal of metal ions from aqueous solutions).

Biomedical Applications

MNPs are developed for a variety of biological and medical applications. The size of the MNPs can range from a few nm to several μm – this makes them compatible with a large variety of biological systems, such as proteins (few nm) to cells and bacteria (few μm).

Most common requirement:
MNPs should be stable in aqueous solution at neutral pH values
$\rightarrow$ magnetite (Fe_3O_4) and maghemite (γ-Fe_2O_3) are typically used as biofunctionalized MNPs.

Basic approach:

- biochemistry enables selective binding of particles
- magnetism allows for easy manipulation and detection:
  - magnetic field gradients can be used to apply force to MNP
  - Most biological systems show only weak dia- or paramagnetism
    $\rightarrow$ magnetic moment of ferromagnetic nanoparticles is easily detectable with little noise in biological environment.

Controlled Manipulation and separation of biological systems:

Bind MNPs to biological systems of interest $\rightarrow$ manipulate biological material via an applied magnetic field gradient. This is used e.g. for separating red blood cells from blood or cancer cells for bone marrow. Other applications include the drug delivery to destination controlled by magnetic field gradients.

Biological sensors:

Well established are DNA microarrays together with fluorescent markers for detection of specific biological molecules. The DNA is bound to a fluorescent molecule and then exposed to an array with many different well-defined DNA strands → will only stick to complementary matching DNA in the array – light signal from the fluorescent marker is used to image location of DNA within the array.

Alternative approach with MNPs:
tag DNA with MNP or fill viruses with MNPs to create 'magnetic viruses' (Fig. 4.16)
→ identify location of bound DNA or 'magnetic viuses' in the array by detection of magnetic stray field from MNP.

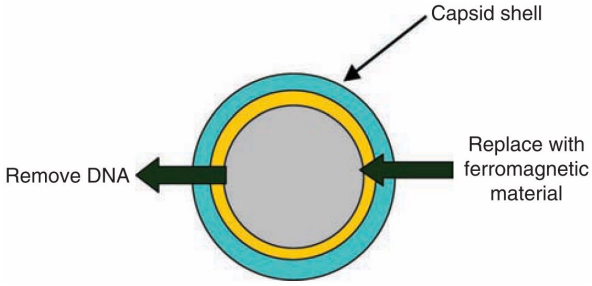

Fig. 4.16: Magnetic virus: The DNA is removed from the virus interior, which results in a rigid empty protein shell. This shell can be used as a template for ferromagnetic nanoparticles. From [Hornyak et al., 2009].

Advantages of MNPs vs fluorescent molecules:
• long-term stability of MNPs; fluorescent markers often degrade with time
• magnetoelectronic sensing of MNPs enables complete electronic readout
• by applying magnetic field gradients, magnetic tags can be used for controlled manipulation of the position of the target molecules (e.g. move towards magnetic field sensor

Hyperthermia:

Basic principle: Rf or microwave irradiation generates heat in the tumor

Problems:
- difficult to heat tumor at deep locations
- selective heating of tumor (not the surrounding tissue)
- ferromagnetic thermoseeds:
  not yet established in clinical use due to problem of unreliable rise in temperature

Current research:
Heating of high-resistivity magnetic oxide materials in external ac magnetic fields
→ loss processes during reorientation of magnetization.

Multi-domain particles:
Hysteresis losses dominate; those depend on the type of magnetization reversal process (domain wall motion or rotational processes).

Single-domain particles:
Magnetization reversal processes (Néel relaxation by thermal activation) depend strongly on temperature and measurement frequency (superparamagnetic behavior of the particle ensemble).
In the case of ferrofluids, also losses due to rotational Brownian motion of magnetic particles may be important

⇒ More research is required to provide better understanding and control.

4.4.3 Magnetic Nanowires

The behaviour of magnetic nano systems becomes much more complex if their shape deviates from a simple spherical geometry, in particular for nano wires, nano tubes and nano discs.

Since there is a non-vanishing contribution of the shape anisotropy, the formation of domain structures and the nature of magnetization reversal processes differs from those of spherical MNPs.

As an example, we consider here the behaviour of nano wires. We analyse the reversal of the magnetization $\boldsymbol{M}$ in an external magnetic field $\boldsymbol{H}$.

Assuming that the magnetization $|\boldsymbol{M}| = const$ is homogeneous within the wire, we can again apply the **Stoner-Wohlfarth model**, but now we have to take into account the shape anisotropy.

If θ is the angle between the magnetization direction and the easy axis (cylinder axis along z-direction; Fig. 4.17), and if we use the demagnetization factors of an infinitely long cylinder, we obtain $N_x = N_y \equiv N_\perp = 1/2$ and $N_z \equiv N_{||} = 0$. Then, the shape anisotropy contribution is derived from Eqs. (4.10) and (4.12) as

$$E_{sh} = \underbrace{\frac{\mu_0}{4} M_s^2}_{\equiv K_{sh}} V \sin^2(\theta) \quad . \tag{4.41}$$

At this point we additionally take into account a magneto-crystalline anisotropy $E_{mc} = K_{mc} \sin^2(\theta)$. Hence, we have now two contributions to the anisotropy energy which can be combined via the definition $K_1 \equiv K_{mc} + K_{sh}$. Hence, the total energy is again given by Eq. (4.36) as

$$E = K_1 V \sin^2(\theta) - \mu_0 H M_s V \cos(\theta - \phi) \quad , \tag{4.42}$$

with the angle ϕ between the direction of $\boldsymbol{H}$ und the easy axis (cylinder axis; Fig. 4.17).

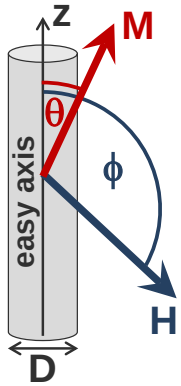

Fig. 4.17: Magnetic nanowire: definition of angles θ and ϕ between the easy axis (z axis) and $\boldsymbol{M}$ and $\boldsymbol{H}$, respectively.

The analysis of Eq. (4.42) – in analogy to the analysis of a spherical particle – provides the switching field H_{sw}. For the case $K_{sh} \gg K_{mc}$, i.e. $K_1 \approx K_{sh}$, and with $\phi = \pi$ (field along the wire axis) the switching field $H_{sw} = H_a \approx 2K_{sh}/(\mu_0 M_s) = M_s/2$.

Alternative model for the reversal of the magnetization: **Curling**

The uniform (spatially homogeneous) rotation of the moments in a nano wire generates a relatively large contribution to the shape anisotropy energy.

The analysis for an infinitely long cylinder with diameter $D > D_{cr}^{curl} = 5.2\, l_{ex}$ within the micromagnetic model shows that a non-uniform reversal of the moments in the 'curling-mode' is the energetically most favourable process. Here, the magnetization is tangentially aligned along the cylinder surface, which reduces E_{sh} (see Fig. 4.18). For an external field H along the cylinder axis, this reversal mechanism provides a switching field

$$H_{sw} = a \cdot \frac{M_s}{2} \quad \text{with} \quad a \equiv 6.78 \left(\frac{2 l_{ex}}{D} \right)^2 \quad . \tag{4.43}$$

For the case $D > D_{cr}^{curl}$ one finds $a < 1$, i.e., the switching field for curling is reduced as compared to the switching field for uniform reversal (Stoner-Wohlfarth).

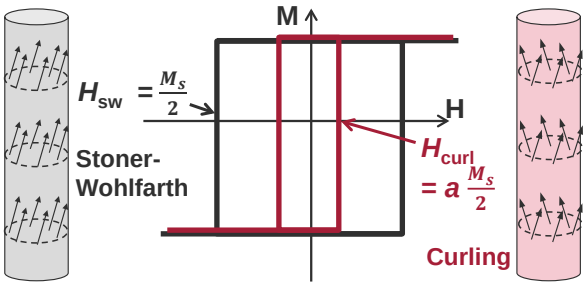

Fig. 4.18: Stoner-Wohlfarth versus curling model for the magnetization reversal of nanowires: Schematic $M(H)$ curves and the orientation of the moments during reversal.

Experiment on a Fe nanowire:

For the measurement of the magnetization of a Fe nanowire (diameter $D_{Fe} = 39\,\text{nm}$), embedded in a carbon nanotube (CNT), the nanowire has been mounted onto a $YBa_2Cu_3O_7$ (YBCO) nanoSQUID [Fig. 4.19(a)]. The magnetic flux Φ, that is coupled from the nanowire into the nanoSQUID, is proportional to the magnetization M of the nano wire.

The diameter of the iron nano wire is $D = 39\,\text{nm} > D_{cr}^{curl} \approx 20\,\text{nm}$. This means that we expect a magnetization reversal by curling. The measurement of the $M(H)$ hysteresis loop [Fig. 4.19(b)] yields a switching field $\mu_0 H_{sw} = 101\,\text{mT}$. The calculated switching field H_{sw} from Eq. (4.43) for curling, with $M_{s,Fe} = 1.71\,\text{kA/m}$ ($\mu_0 M_{s,Fe} = 2.2\,\text{T}$) yields $H_{sw} = 103\,\text{mT}$ (with $a = 0.0955$). This is in excellent agreement with the experiment.

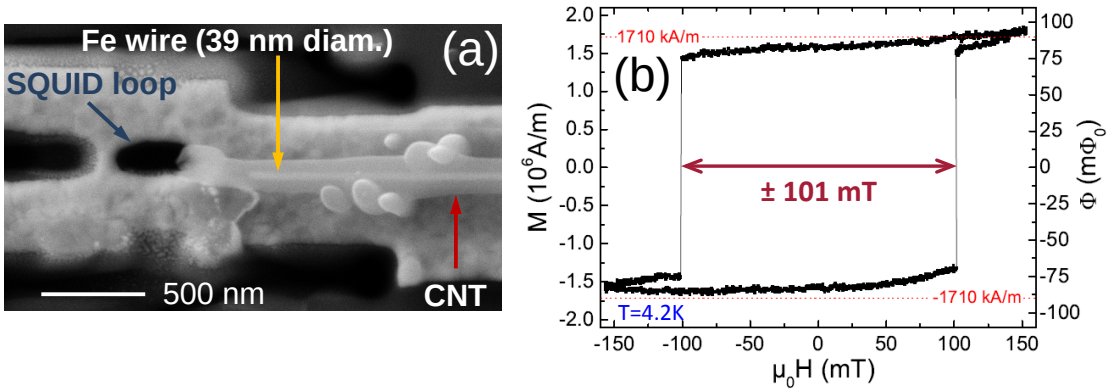

Fig. 4.19: Fe nanowire in a carbon nanotube (CNT) on top of a YBCO nanoSQUID: (a) SEM-image; (b) $M(H)$ hysteresis loop (right axis shows magnetic flux signal), measured with the nanoSQUID at $T = 4.2\,\text{K}$. Horizontal dotted lines indicate the literature value of M_s. From [Schwarz et al., 2015].

4.5 Magnetism of Thin Films and Multilayers

In the following we consider the electric transport properties of ferromagnetic layer systems and devices with non-magnetic interlayers or insulating tunnelling barriers. Here, *spin-dependent scattering* and *spin-dependent tunneling* play an important role. We start with some introductory remarks on the field of spintronics in Sec. 4.5.1. After that we will discuss giant magnetoresistance (GMR) in Sec. 4.5.2, and tunneling magnetoresistance (TMR) in Sec. 4.5.3.

4.5.1 Magnetoelectronics / Spintronics, 'MR effects'

Until the late 1980's, magnetism and electronics were to a large extent the subjects of independent fields of research. However, there was one important common field of application in **data processing** and **data storage**.

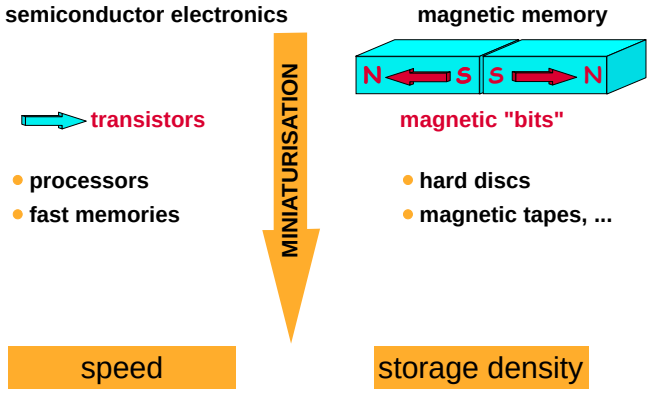

Fig. 4.20: Data processing and storage as a common field of application for semiconductor electronics and magnetism. For long time, the technological developement within these fields was essentially independent.

Continuous further developements in the miniaturization of magnetic structures (e.g. ultrathin films) revealed surprising new effects with respect to their magnetic *and* electric properties.

⇒**spintronics:** exploits the fact that electrons carry a magnetic moment (which is coupled to a spin) in addition to electric charge

electrons = carriers of electric charge and spin

Most important effects: **magnetoresistance (MR) effects**
⇒ developement (since the 1990's) of the so-called **XMR-technologies** (X: any)

Obvious application:
Transformation of magnetic information into electric information in **sensorics, magnetic storage technologies** (well established), or for novel device concepts, e.g. **spin-transistors**.

Definition: **magnetoresistance**[10] (R: electrical resistance, H: magnetic field)

$$MR \equiv \frac{R(H) - R(0)}{R(0)} = \frac{\Delta R}{R(0)} \tag{4.44}$$

[10] One distinguishes (i) *positive MR*, i.e., increase of R with H and (ii) *negative MR*, i.e., reduction of R with H. The lattter is often normalized to $R(H)$, i.e., $MR > 100\,\%$ is possible !!

Until the end of the 1980's:

Only in special cases (e.g. quantum hall effect), the electrical properties of solids – in particular the electric resistance R – can be significantly manipulated by applying external magnetic fields. Well established MR effects at that time are:

i) *positive MR effect*:

In *non-magnetic metals* (e.g., Au, Ag, Cu), an applied field H causes a reduction of the effective mean free path of the charge carriers in a solid (due to the Lorentz force) and hence a slight increase of R, scaling as $\Delta R \propto H^2$. However, $MR \ll 1\%$ in $\mu_0 H \approx 1\,\mathrm{T}$; i.e. not useful for applications

ii) *anisotropic MR effect (AMR)*:

In *ferromagnetic metals* (e.g. permalloy Fe_xNi_{1-x}), the resistance R depends on the direction of current relative to H, i.e., $R(H_{||I}) \neq R(H_{\perp I})$ (see Fig. 4.21). This yields MR values up to a few %, with first applications in read heads for hard discs.

⇒ low interest in MR effects since they are too small for many applications

New developements since the late 1980's:

Discovery of MR effects that are based on the dependence of electric transport properties on the spin orientation of charge carriers. The spin orientation can be manipulated by an external magnetic field H (see Fig. 4.21).

- *Giant* MR effect (GMR)
  – 1988 by Grünberg and Fert (Nobel prize in physics in 2007)
  [Baibich et al., 1988, Binasch et al., 1989]
  → magnetic coupling & **spin-dependent scattering** in multilayer structures, i.e., thin films made from magnetic and non-magnetic (metallic) layers

- *Colossal* MR effect (CMR)
  – 1993 [von Helmolt et al., 1993] [11]
  → complex interplay between structural, magnetic and orbital order (in mixed-valence Mn oxides)

- *Tunneling* MR effect (TMR) at room temperature (R.T.)
  – 1995 [Moodera et al., 1995] [12]
  → **spin-dependent** (spin polarized) **tunneling** of electrons, spin injection

⇒ efficient change of the resistance of a solid in magnetic fields (at R.T.) up to several 10 % for GMR, $> 100\,\%$ for TMR and up to $> 10^5$ for CMR

- huge application relevance of GMR and TMR

[11] Already in 1950 J. H. van Santen and G. H. Jonker [Van Santen and Jonker, 1950] discovered the CMR effect in perovskite-based manganites; however, only at low temperatures. The discovery of CMR in thin films at room temperature by R. von Helmolt *et al.* triggered strong scientific interest.

[12] This effect was already discovered and described by Julliere in the 1970's [Julliere, 1975], but only at low temperatures. For a long time it was not reproducible.

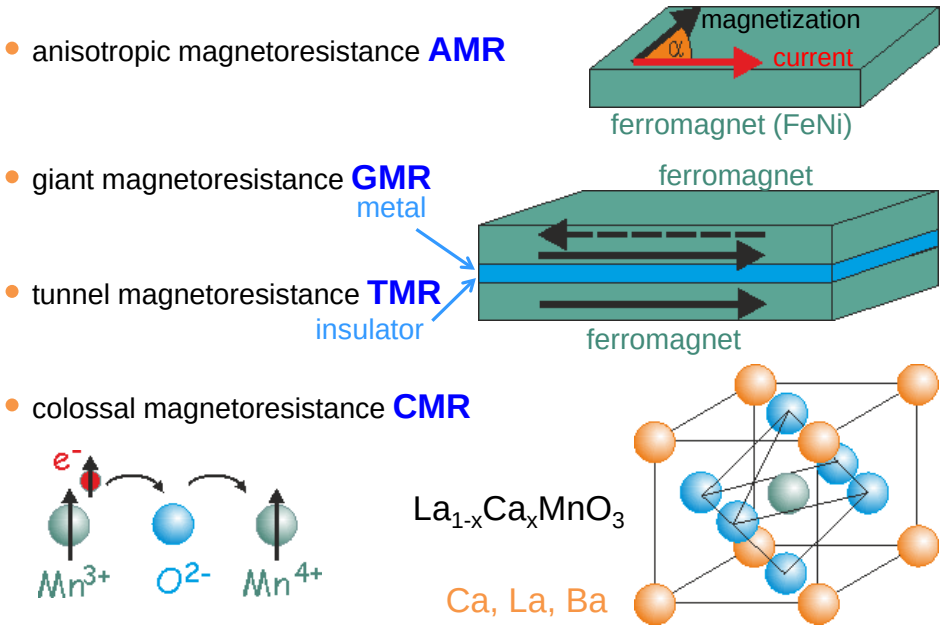

Fig. 4.21: overview over MR effects

Fields of application:

i) Sensorics

Changes ΔH in magnetic field serve as an indicator for magnetic, electric or mechanical parameters, that are converted into an electric signal and then further processed with conventional electronics.

- analog sensors: rotation sensors, position measurement, ...
→ vehicle construction, mechanical engineering, medical technology, smart phones

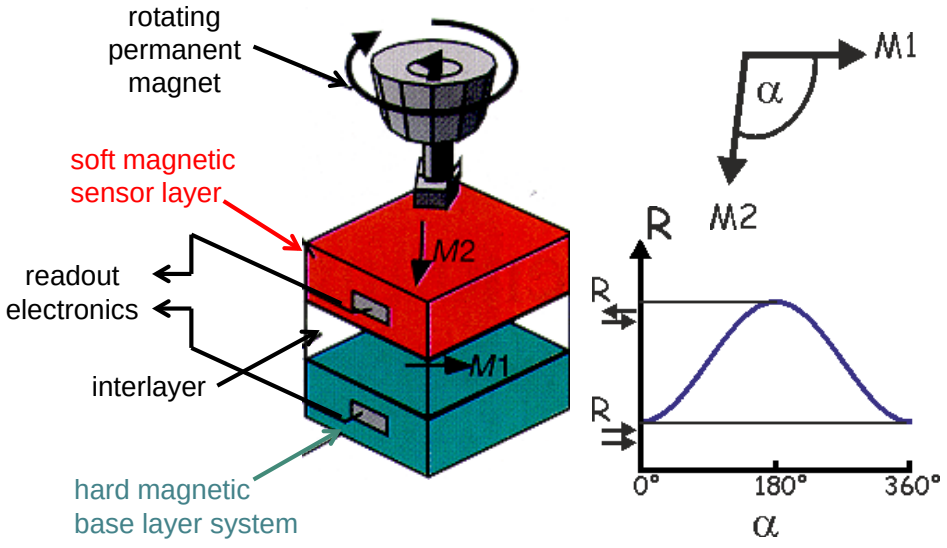

Fig. 4.22: Magnetoresistive rotation sensor

Advantages:
- can be miniaturized → low costs
- contact-free measurements in robust environment
- simple read-out electronics

- digital sensors: hard disc read heads

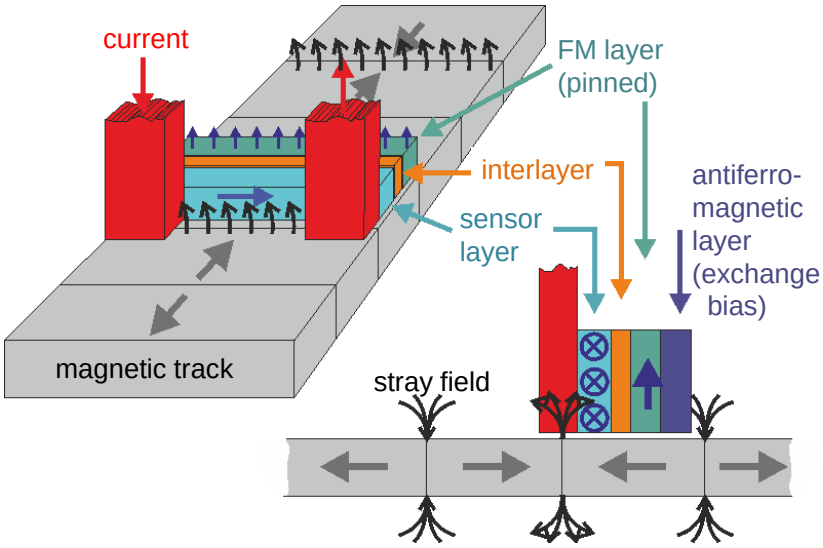

Fig. 4.23: GMR read head: schematic layout and working principle

significant advantage: can be extremely miniaturized
→ read out suitable for high storage densities

⇒ only a few years after the discovery of the GMR effect, this has lead to a dramatic increase of the storage capacity of hard discs.

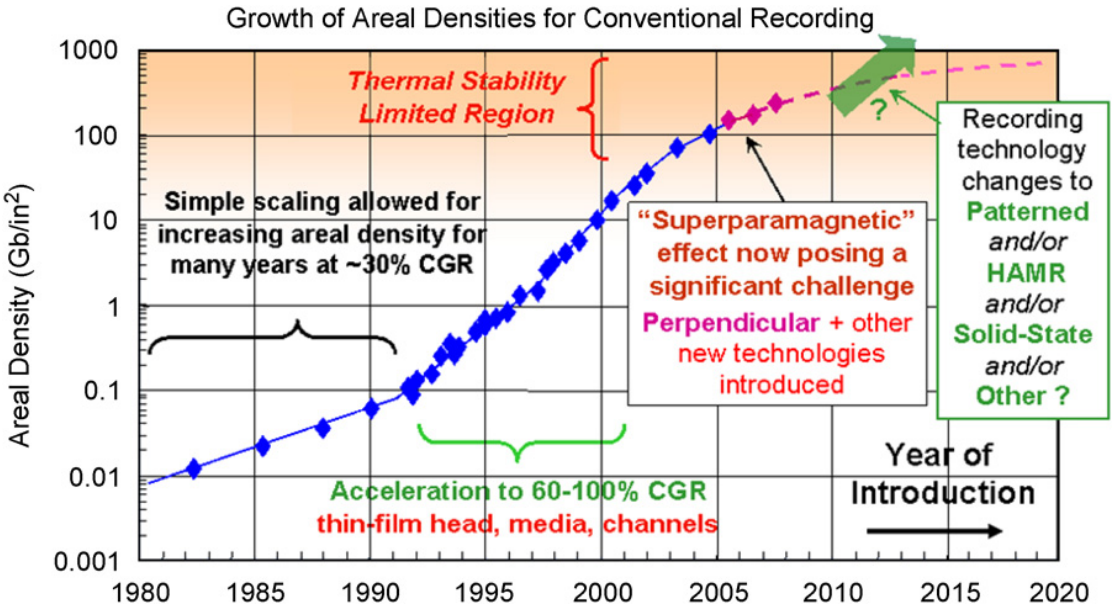

Fig. 4.24: Chronological developement of the storage capacity of hard discs; the strong rise with annual growth rates (CGR='compound growth rate') $> 50\,\%$ since the beginning of the 1990's until ∼2005 is based on the developement of MR sensors; from [Wood, 2009].

(ii) non-volatile memories (MRAMs)

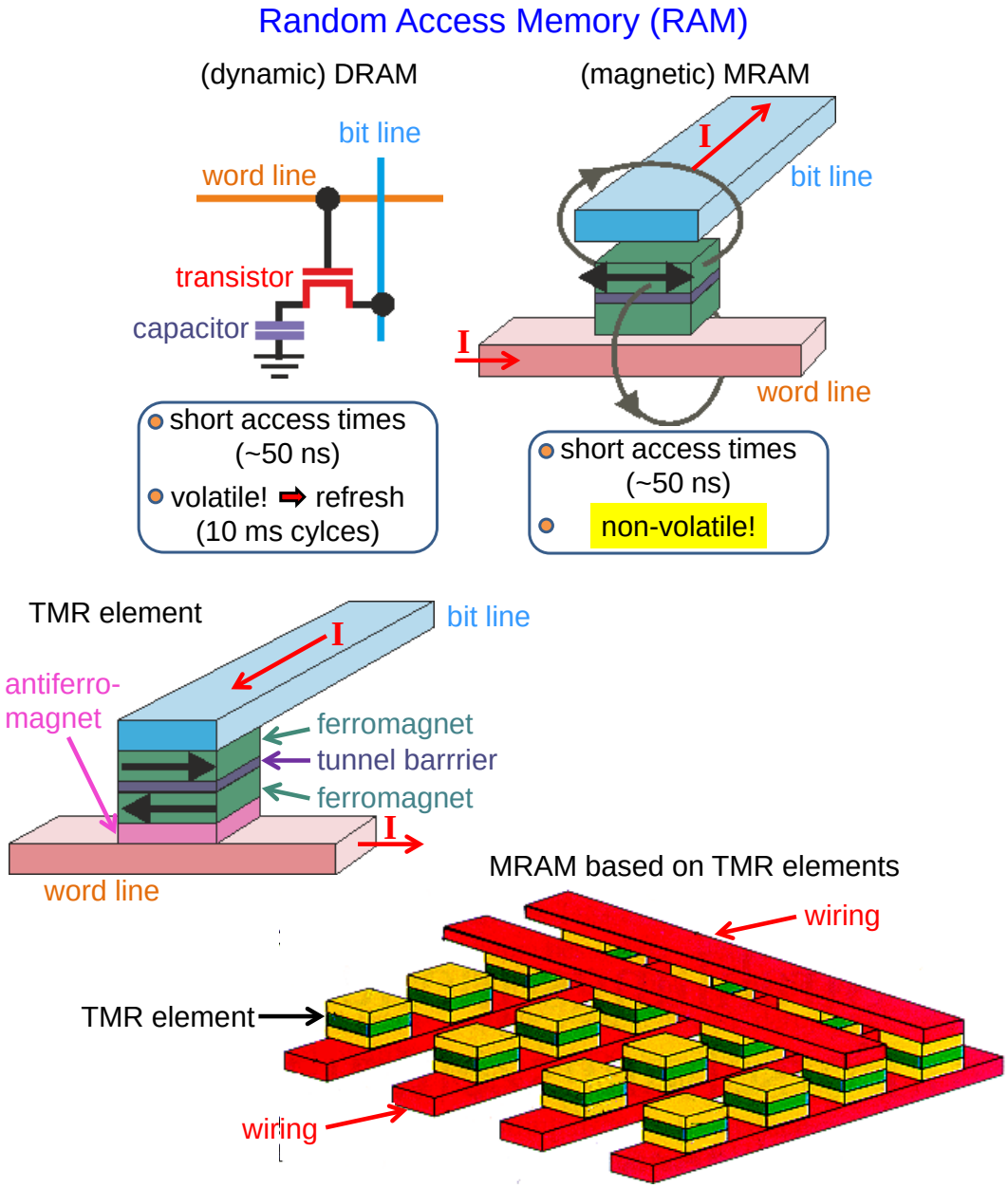

Fig. 4.25: Magnetic Random Access Memory (MRAM) in comparison with DRAM.

are based on TMR effect; have enormous commercial application potential

advantages:
- lower power consumption (Laptops)
- non-volatile (avoids 'booting')
- fast (comparable to DRAM)
- can be miniaturized (which promises enormously huge storage densities)

Conclusion

Enormously fast transition from basic research to important future technologies. This means that close interaction of basic research and technological developement makes MR effects/XMR technologies highly attractive.

4.5.2 Giant Magnetoresistance (GMR)

The GMR appears in **layer systems** consisting of ferromagnetic metals (**F**), which are seperated by thin, non-magnetic metals (**N**).

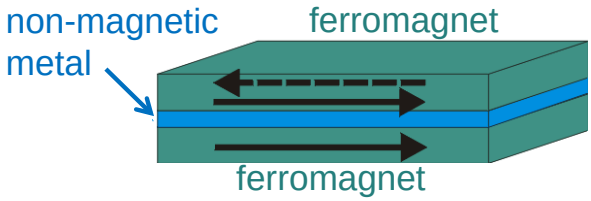

Fig. 4.26: Schematic representation of a GMR structure; the arrows indicate the orientation of the magnetization **M** in the two F layers.

Example: Co/Au/Co or Fe/Cr/Fe

An **antiparallel (a)** alignment of the **magnetization** $\boldsymbol{M}$ of the F layers is transferred into a **parallel (p)** alignment by applying a magnetic field.

⇒ **strong decrease of the resistance**
does not dependend on the direction of the current ('in-plane' or $\perp$) and on the orientation of the current with resepect to the magnetic field (different from AMR mechanism)

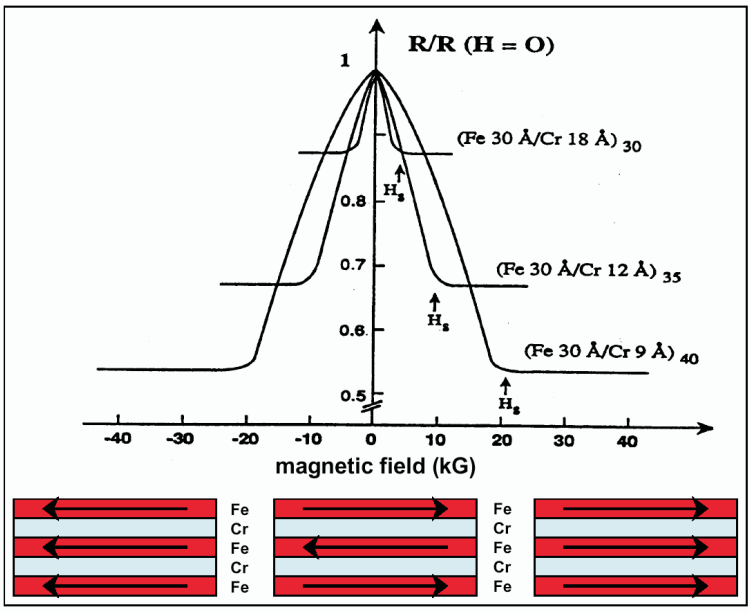

Fig. 4.27: Magneto-resistance of Fe/Cr layer structures at 4.2 K. One observes a maximum magneto-resistance for a Cr layer thickness of 0.9 nm. For this layer thickness, in the field-free case, there is antiparallel coupling of the magnetization. Adapted from [Baibich et al., 1988].

Conventional **definition** of the GMR effekt: $GMR = \frac{R_a - R_p}{R_p}$
(with resistance R_a for antiparallel and R_p for parallel $\boldsymbol{M}$ in adjacent F layers)

Record value in **multilayer systems**: >200 % at 4.2 K; up to 80 % at 300 K

Explanation within the two-channel-model:

Is based on the description of N. F. Mott for spin-dependent scattering in transition metals [Mott, 1964]:

- electric current is mainly carried by electrons of the s band.
→ high mobility due to small effective mass (band curvature)
- electric resistance is mainly determined by the scattering of these s electrons into unoccupied states in the d band.

High density of states in the d band at E_F $\Rightarrow$ high scattering rate $\Rightarrow$ high resistance

in the ferromagnetic state ($T < T_C$), the exchange interaction leads to a splitting of the **sub-bands for minority spins** (spins antiparallel to **M**) **and majority spins** (spis parallel to **M**); see Fig. 4.28, left.

$\rightarrow$ spin dependent scattering for spin-$\downarrow$- und spin-$\uparrow$electrons

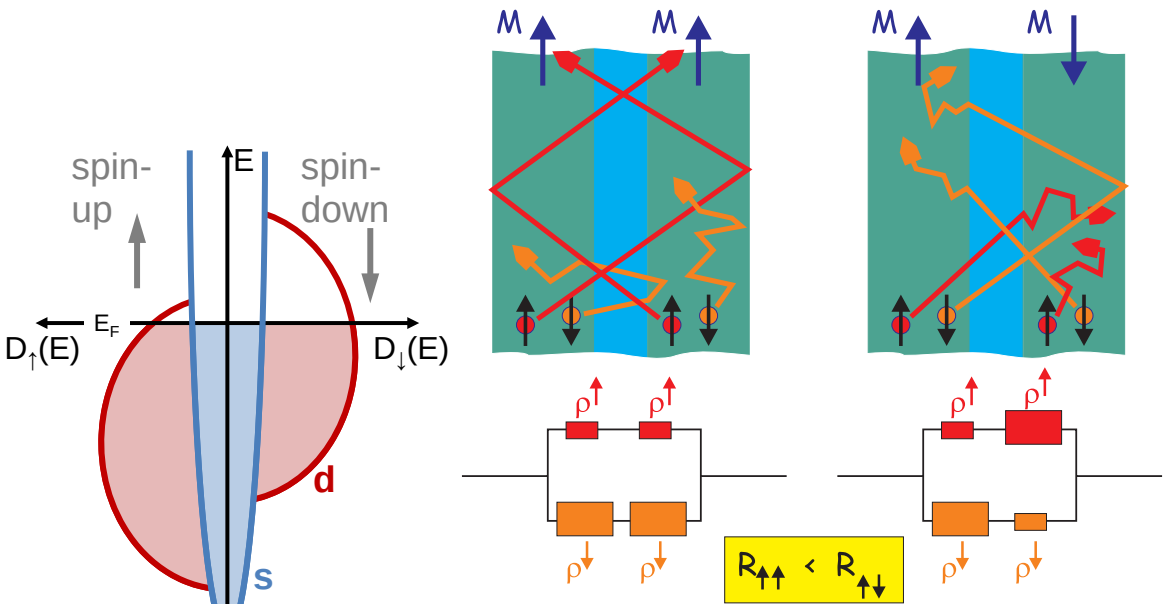

Fig. 4.28: **Left:** Exchange splitting causes different density of states $D(E)$ at the Fermi level E_F for spin-$\uparrow$und spin-$\downarrow$electrons. **Right:** GMR effect in the framework of the two-channel-model.

Consider GMR structure in Fig. 4.28(right), consisting of two F layers, seperated by an N layer.

In case of an increased scattering rate of the minority charge carriers:

i) parallel **M**: in both F layers:
strong scattering of the minority charge carriers (large ρ)
and weak scattering of the majority charge carriers (small ρ)

$\rightarrow$ dominant contribution of the higher conductivity of the majority charge carriers (in both F layers) to the total resistance $R_{\uparrow\uparrow}$

ii) antiparallel $\boldsymbol{M}$: each spin orientation yields a combination (series connection) of large and small ρ in both F layers.

$\rightarrow$ parallel connection of both (equivalent) spin channels with intermediate value of ρ in each case gives total resistance $R_{\uparrow\downarrow}$

Comparison of both configurations yields $R_{\uparrow\uparrow} < R_{\uparrow\downarrow}$

Note:

A detailed description and explanation of the GMR is much more complex.
One distinguishes between extrinsic GMR (describend within the above two-channel-model) and intrinsic GMR (includes the particular band structure of the systems).
Furthermore, the scattering at the F-N boundary plays an important role.

Realization of antiparallel alignment of M in adjacent F layers:
(in zero-field, or in low fields in the mT range)

- antiferromagnetic **interlayer exchange coupling**: magnetic coupling between adjacent F layers favours – for certain values of thickness d_N of the N layer – an antiparallel alignment of the magnetization $\boldsymbol{M}$ of the layers at $H = 0$.

- **'spin valves'**: Pinning of one of the two F layers by coupling to an antiferromagnetic (AF) layer (e.g. FeMn) → **exchange anisotropy** (*exchange bias* = EB) at the F/AF interface shifts $M(H)$ hysteresis loop of the pinned F layer by H_{EB}

Interlayer exchange coupling (IEC)

F/N/F trilayers show – in zero field – an alternating **antiparallel** and **parallel** alignment of $\boldsymbol{M}$ of the two F layers, as a function of the thickness d_N of the non-magnetic interlayer (N), if the N-layer thickness is only a few monolayers.

Measurements on wedge-shaped samples:

- thickness of the two F layers (Fe)=const.; thickness of the N layer (Cr) varies.

Measurement: electric transport $R(H)$ and magneto-optical Kerr-effect (MOKE)[13]: Rotation of the polarization plane of reflected light provides a direct measure of the (local net) magnetization of both F layers. The change of the magnetic structure due to IEC yields **characteristic domain patterns**, which can be observed by MOKE.

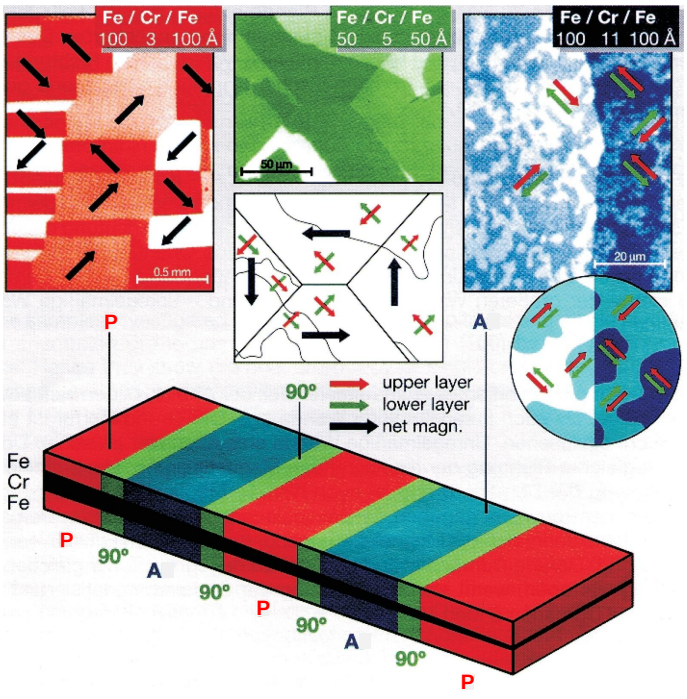

Fig. 4.29: MOKE images of domain patterns in a Fe-Cr-Fe layer system with wedge-shaped Cr layer show different types of magnetic coupling, depending on the thickness of the Cr layer. The magnetization directions of the two F layers can be parallel (p), antiparallel (a) or they can be rotated by 90 ° with respect to each other. Arrows indicate the magnetizations of the upper layer (red), lower layer (green) and the net magnetization of both layers (black). from [Grünberg, 1995].

Minimization of the domain wall energy leads to straight domain walls if the net magnetization of both layers rotates across a domain wall – this is the case for parallel coupled layers, but not for antiparallel coupled ones (where the net magnetization is always zero) → allows to distinguish between parallel (p) and antiparallel (a) coupling (also 90 °-coupling) in MOKE-images.

[13] For the description of MOKE, see e.g. [Hubert and Schäfer, 1998].

GMR effect in spin valves

The antiferromagnetic interlayer exchange coupling (in zero-field) is not a necessary condition for the occurence of the GMR effect.

Crucial is:
Variation of the applied magnetic field allows switching between parallel and antiparallel alignment of the magnetization of adjacent F layers.

Possible realizations:
Combination of F layers with **different coercive fields** $\boldsymbol{H}_{\mathbf{coerc}}$, like e.g. $Co/Au/Ni_{80}Fe_{20}$.

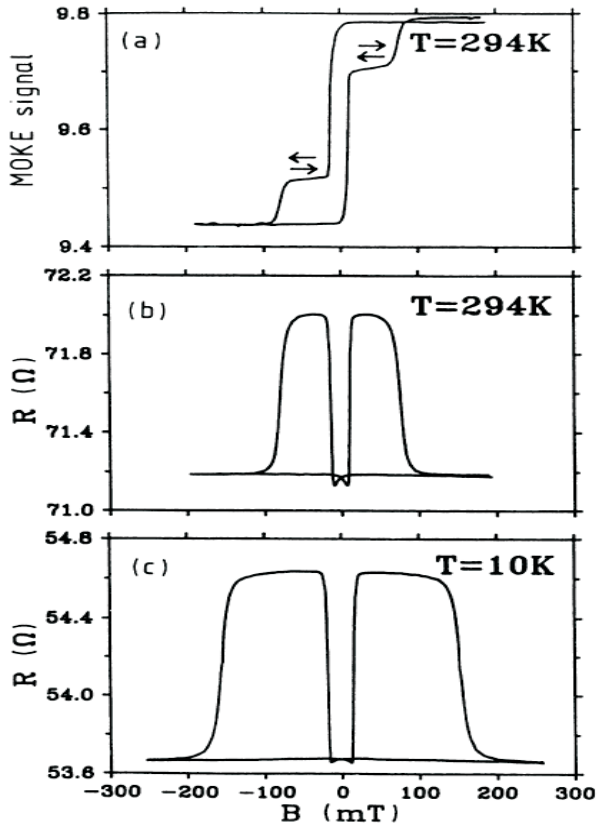

Fig. 4.30: Measurement on a Co/Au/Co layer structure (d_{Co} = 10 nm, d_{Au} = 6 nm): MOKE-signal (a) and $R(B)$-curves at 294 K (b) and at 10 K (c). H_{coerc} of the Co layer on a [110] GaAs-substrate is larger due to stronger strain in comparison with the Co film on the Au interlayer. From [Barnas et al., 1990].

Spin valves[14] based on exchange anisotropy:

for technical applications nowadays widely used:

- magnetically soft layer (F1, 'free')
- seperated by non-magnetic layer (N) from
- second, 'pinned' magnetic layer (F2, 'pinned').

'Pinning' of the magnetization of the F2 layer by coupling to an antiferromagnetic (AF) layer via **exchange anisotropy** (*Exchange Bias*)[15] – shifts $M(H)$ hysteresis loop along the H axis.

Materials are for e.g. NiFe (F) / Cu (N) / NiFe (F) / FeMn (AF)

[14] The term 'spin valve effect' has been introduced by [Dieny et al., 1991].
[15] See e.g. the review article by [Schuller, 2004].

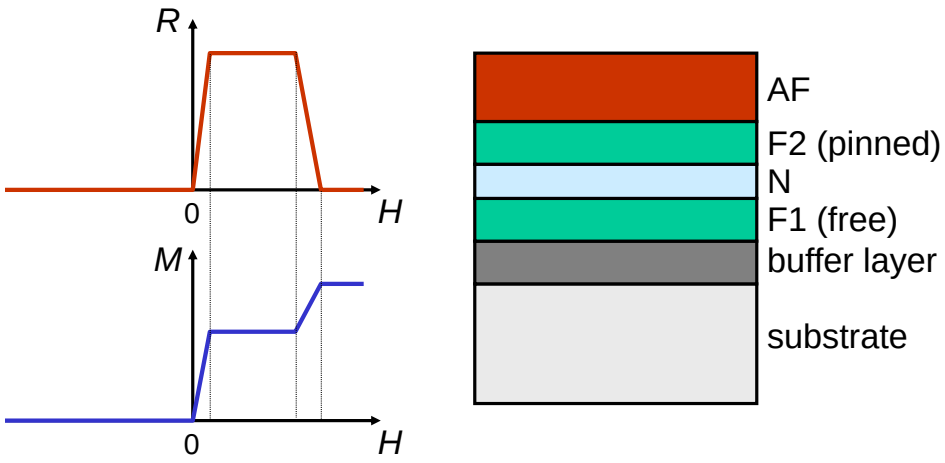

Fig. 4.31: Schematic representation of the magnetic field dependence of magnetization and resistance (left), and the basic layer structure of a spin valve (right).

$R(H)$ and $M(H)$:

- increase of H from negative to positive values
→ near $H = 0$ the first, soft magnetic layer(F1, free), switches;
magnetization of the F2-layer (pinned) stays the same
⇒ strong increase of the resistance,
since magnetization of both F layers is now antiparallel.

- further increase of H:
R remains high until the external field becomes so strong,
that the exchange coupling is overcome
→ magnetization of the pinned F2 layer switches
⇒ resistance decreases

Advantages of spin valves:

- simpler technology
(thicker N layers are possible; as long as $d_N <$ spin diffusion length in the N layer)

- large slope of $R(\mu_0 H)$ at low fields (typical $> 30\,\%/\mathrm{mT}$),
- good linearity and free from hysteresis

→ utilisation for many low-field applications (H sensors, read heads for hard discs)

Note:
Many experiments on GMR show that this effect always occurs when ferromagnetic (F) regions are seperated by thin, non-magnetic (N) regions.

'Thin' means: conduction electrons can cross the N area without spin-flip scattering.

4.5.3 Tunnel magnetoresistance (TMR)

We consider trilayer systems composed of two ferromagnetic (F) thin films, which are seperated by a very thin, insulating (I) layer:

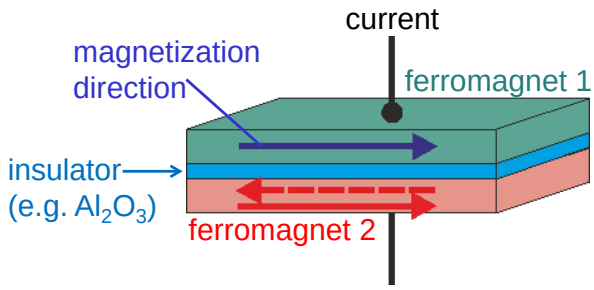

Fig. 4.32: Schematic representation of a magnetic tunnel junction which consists of a F/I/F trilayer structure.

If the thickness of the insulating layer is small enough, there is a finite probability for the quantum-mechanical tunneling of the charge carriers through the insulating barrier – in so called **F/I/F tunnel junctions**.

Based on fundamental experimental work on the **spin-conservation during the tunneling process** of the electrons, and on the **spin polarization of the conduction electrons in ferromagnets** at the beginning of the 1970's [Meservey et al., 1970, Tedrow and Meservey, 1971], Julliere developed a quantitative model [Julliere, 1975], which predicts that tunneling in F/I/F junctions should lead to a very high magnetoresistive effect, the so callend *tunneling magnetoresistance (TMR)*.

TMR is based on the fact that the tunnel current depends on the relative orientation of the magnetization direction of the two F electrodes.

Definition for TMR effect: $TMR \equiv \frac{R_a - R_p}{R_p}$ (as for GMR)

Spin polarization

For an understanding of the TMR effect, the lifting of the degeneracy of the density of states $D_\uparrow(E_F)$ for the spin-↑-electrons and $D_\downarrow(E_F)$ for the spin-↓-electrons at the Fermi level E_F for both F layers plays an essential role.

While in Cu the density of states for spin-up and spin-down electrons is symmetric, for Fe, Co and Ni $D_\uparrow(E_F) \neq D_\downarrow(E_F)$ (Fig. 4.33).

We define $m \equiv D_{maj}(E_F)/[D_{maj}(E_F) + D_{min}(E_F)]$ as the fraction of the electronic states at the Fermi level with spin orientation in the direction of the magnetization (majority spins). Accordingly, $(1-m) \equiv D_{min}(E_F)/[D_{maj}(E_F) + D_{min}(E_F)]$ is the fraction of the electronic states at the Fermi level with spin orientation opposite to the direction of the magnetization (minority spins).

The **spin polarization** P is then defined als the difference of these fractions

$$P \equiv \frac{D_{maj}(E_F) - D_{min}(E_F)}{D_{maj}(E_F) + D_{min}(E_F)} = m - (1-m) = 2m - 1 \quad . \tag{4.45}$$

This means that the spin polarization describes the asymmetry in the density of states for spin-↑ and spin-↓ electrons **at the Fermi-level**.

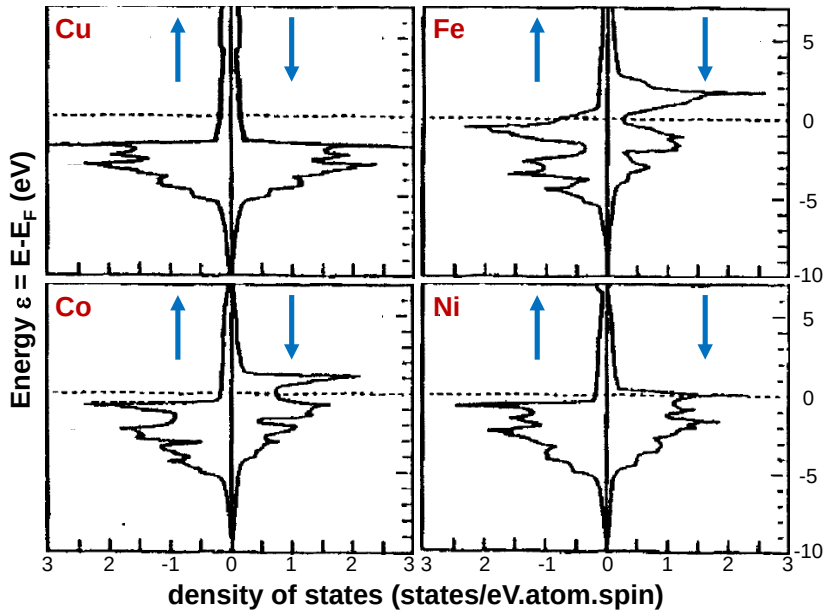

Fig. 4.33: Density of states for majority- and minority-electrons in ferromagnetic Fe, Co, Ni in comparison with non-magnetic Cu. Horizontal dashed lines indicate Fermi level. Modified from [Moodera et al., 1999].

The fraction m can assume values within $0 \leq m \leq 1 \Rightarrow -1 \leq P \leq +1$
$\rightarrow$ **different sign of the spin polarization** possible.

As shown in Fig. 4.33, the spin-$\uparrow$electrons in Fe (here: majority spins) have a larger density of states than the spin-$\downarrow$electrons (here: minority spins) $\rightarrow P > 0$.
In Co and Ni, however, this is just reversed $\rightarrow P < 0$

Typical values in 3d transition metals: $|P|$ several 10 %

Julliere model for F/I/F junctions

$\rightarrow$ simple model for the tunnel conducance of F/I/F junctions [Julliere, 1975].
$\rightarrow$ for the analysis of the magnetoresistive effect in Fe/Ge/Co junctions at $T = 4.2\,K$ which was first observed by Julliere

The Julliere model makes the following **assumptions** for the tunnel process:

- elastic tunneling (no change of the energy of the electrons)
- spin conservation (no spin-'flips')
- the tunnel conductance $G \equiv \partial I/\partial U$ for each spin direction is proportional to the densitiy of states $D(E_F)$ of each spin direction (at the Fermi level) in both electrodes $i = 1, 2$:
  $G_\uparrow \propto D_{1,\uparrow}(E_F)D_{2,\uparrow}(E_F)$, and $G_\downarrow \propto D_{1,\downarrow}(E_F)D_{2,\downarrow}(E_F)$.

Within a strongly simplified scheme of the band structure of the d electrons for transition metals, the basic principle of the TMR effect is illustrated in Fig. 4.34 (here for identical electrodes with $P < 0$, i.e. with $D_{maj}(E_F) < D_{min}(E_F)$):

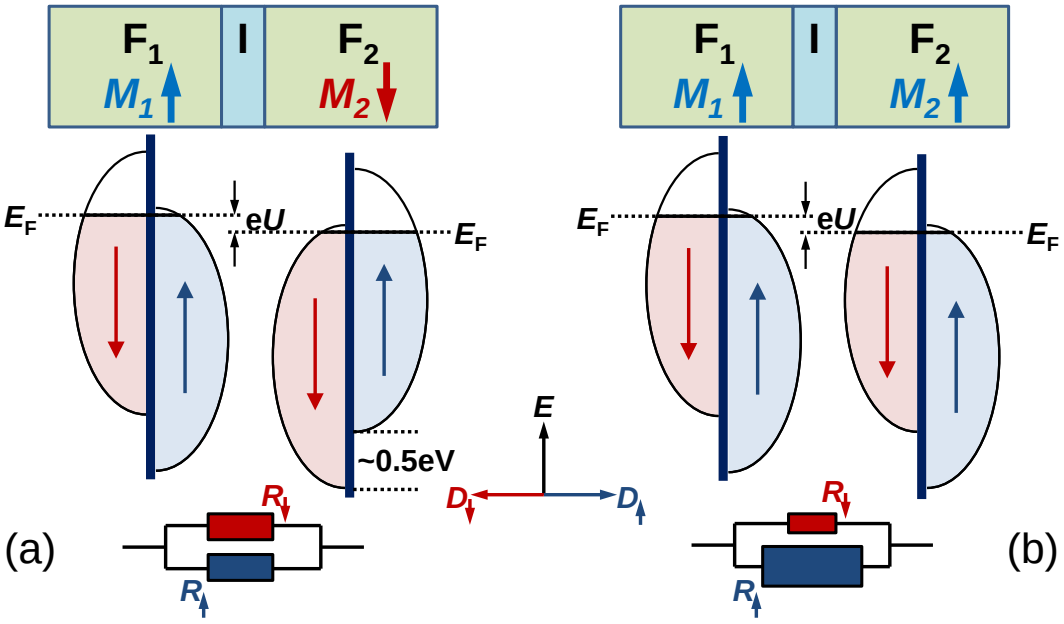

Fig. 4.34: Schematic representation of the density of states $D_\uparrow(E)$ and $D_\downarrow(E)$ of the majority- and minority-spin-states, respectively (top) in a ferromagnetic tunnel junction, with (a) antiparallel and (b) parallel magnetization orientatin of the two F electrodes. Bottom pannels indicate the resulting tunnel resistances.

essential:
-ferromagnetic exchange splitting $\Rightarrow$ finite spin polarization P

- finite voltage U $\Rightarrow$ tunneling from left (occupied states) to the right (unoccupied states)

consider occupied and unoccupied densities of states **at $\mathbf{E_F}$** on both sides:

antiparallel alignment of M:

• many occupied minority spins ($\downarrow$, left)
$\rightarrow$ few unoccupied majority spins ($\downarrow$, right)

• few occupied majority spins ($\uparrow$, left)
$\rightarrow$ many unoccupied minority spins ($\uparrow$, right)

$\Rightarrow$ **parallel tunneling channels** with **equal resistances** $R_\downarrow$ **and** $R_\uparrow$ of intermediate values

parallel alignment of M:

• many occupied minority spins ($\downarrow$, left)
$\rightarrow$ many unoccupied minority spins ($\downarrow$, right)

• few occupied majority spins ($\uparrow$, left)
$\rightarrow$ few unoccupied majority spins ($\uparrow$, right)

$\Rightarrow$ **parallel tunneling channels** with **small resistance** ($R_\downarrow$) und **large resistance** ($R_\uparrow$)

$\Rightarrow$ **tunnel resistance** at M_1 **antiparallel** M_2 ist **larger** than **tunnel resistance** at M_1 **parallel** M_2

From this picture, it is evident that in case of **100% spin polarization** and for **antiparallel** orientation of the magnetatization, the tunnel conductance should even reach zero, i.e. the **tunnel resistance goes to infinity**.

Quantitative analysis of Julliere:

In the following, the densities of states D are always (!!) the densities of states at the Fermi level $D(E_F)$; to simplify the expressions we omit (E_F).

According to the definition (4.45) of the spin polarization P_i of the electrodes $i = 1, 2$ (with the total density of states $D_i \equiv D_{i,maj} + D_{i,min}$ for electrode i):

Fraction of the majority charge carriers: $m_i = D_{i,maj}/D_i = (1 + P_i)/2$

Fraction of the minority charge carriers: $1 - m_i = D_{i,min}/D_i = (1 - P_i)/2$

With this, one obtains for the tunnel conductanc G_p for **parallel alignment of the magnetization directions**
(with M_i in $\uparrow$-direction for both electrodes i, i.e. $D_{i,\uparrow} = D_{i,maj}$ and $D_{i,\downarrow} = D_{i,min}$)

$$\begin{aligned} G_p &\propto D_{1,\uparrow} \cdot D_{2,\uparrow} + D_{1,\downarrow} \cdot D_{2,\downarrow} \\ &= [m_1 m_2 + (1 - m_1)(1 - m_2)] \cdot D_1 D_2 \\ &= \frac{1}{2}(1 + P_1 P_2) \cdot D_1 D_2 \end{aligned} \tag{4.46}$$

and for the tunnel conductance G_a for **antiparallel alignment of the magnetization directions**
(with M_1 in $\uparrow$-direction, i.e. $D_{1,\uparrow} = D_{1,maj}$ and $D_{1,\downarrow} = D_{1,min}$
and M_2 in $\downarrow$-direction, such that $D_{2,\uparrow} = D_{2,min}$ and $D_{2,\downarrow} = D_{1,maj}$)

$$\begin{aligned} G_a &\propto D_{1,\uparrow} \cdot D_{2,\uparrow} + D_{1,\downarrow} \cdot D_{2,\downarrow} \\ &= [m_1(1 - m_2) + (1 - m_1)m_2] \cdot D_1 D_2 \\ &= \frac{1}{2}(1 - P_1 P_2) \cdot D_1 D_2 \end{aligned} \tag{4.47}$$

This yields for the ratio G_p/G_a

$$\frac{G_p}{G_a} = \frac{1 + P_1 P_2}{1 - P_1 P_2} \tag{4.48}$$

From this, we can derive the *tunnel magnetoresistance* **TMR** (with $R = 1/G$):

$$TMR \equiv \frac{R_a - R_p}{R_p} = (\frac{1}{G_a} - \frac{1}{G_p})G_p = \frac{G_p}{G_a} - 1 = \frac{2P_1 P_2}{1 - P_1 P_2} \tag{4.49}$$

For identical electrodes with 100% spin polarization

$$P_1 = P_2 = 1 \;\Rightarrow\quad G_a = 0 \quad \text{i.e.} \quad TMR \to \infty$$

The following technical problems prevented large TMR effects at R.T. until 1995:

- roughness of the ferromagnetic electrodes,
- defective tunnel barriers,
- insufficient quality of the interfaces and
- quality and domain structure of the ferromagnetic electrodes.

More recent experiments on TMR

It took until the mid 1990's – in particular due to improvements of the fabrication technology – when an experimental breakthrough was achieved [Moodera et al., 1995]. This lead to the first achievement of significant TMR values of several 10 % at room temperature. Figure 4.35 shows as an example $R(H)$ measurements on a TMR device using F electrodes (i=1,2) with different coercive fields ($H_{\mathrm{coerc,i}}$).

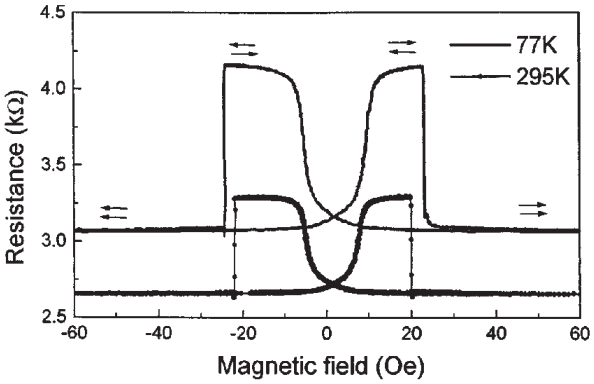

Fig. 4.35: $R(H)$-curves for a Co/Al_2O_3/Permalloy ($Ni_{80}Fe_{20}$) tunnel junction, with TMR=36 % at 77 K and 23 % at room temperature. Arrows indicate the magnetization directions of the two electrodes. From [Moodera et al., 1998].

- start at strong negative field $|H| > |H_{coerc,i}|$:
→**(P)-configuration** of M_i (parallel to applied field) → **low resistance**

- increase of the field until (positive) $H = H_{coerc,1}$
→ reversal of the magnetization M_1 of electrode 1 into direction of the field
→ **(A)-configuration** of M_i → **strong increase of the resistance**

- further increase of the field until $H = H_{coerc,2}$
→ reversal of the magnetization M_2 of electrode 2 into direction of the field
→ **(P)-configuration** of M_i → **strong decrease of the resistance**

By sweeping back the field to the starting value (strongly negative value)
→ mirrored behaviour relative to the $H = 0$ axis ⇒ **strong hystereis**

Materials:

- **3d transition metals** (e.g. Co, Ni, Permalloy) with Al_2O_3-tunnel barrier:
→ TMR up to 40 %

- some **transition metal oxides**
(are semimetals → Fermi level intersects only one of the two 3d bands)
show very large spin polarization up to 100 % at R.T.) → TMR up to ≳100 %

In mixed-valence manganoxides (manganites), huge TMR values up to ∼2000 % at low temperature (∼ 5 K) [see Fig. 4.36(b)]
→ $La_{2/3}Sr_{1/3}MnO_3/SrTiO_3/La_{2/3}Sr_{1/3}MnO_3$ (LSMO/STO/LSMO) tunnel junction [Werner et al., 2011].

Disadvantage: Curie-temperature mostly below room temperture; at best $T_C \sim 360$ K in $La_{1-x}Sr_xMnO_3$ (LSMO) with optimal doping $x \sim 0.35$.

→ stimulated search for other semimetals with higher T_C:
- CrO_2, Fe_3O_4 (magnetite),
- double-perovskite $A_2BB'O_6$

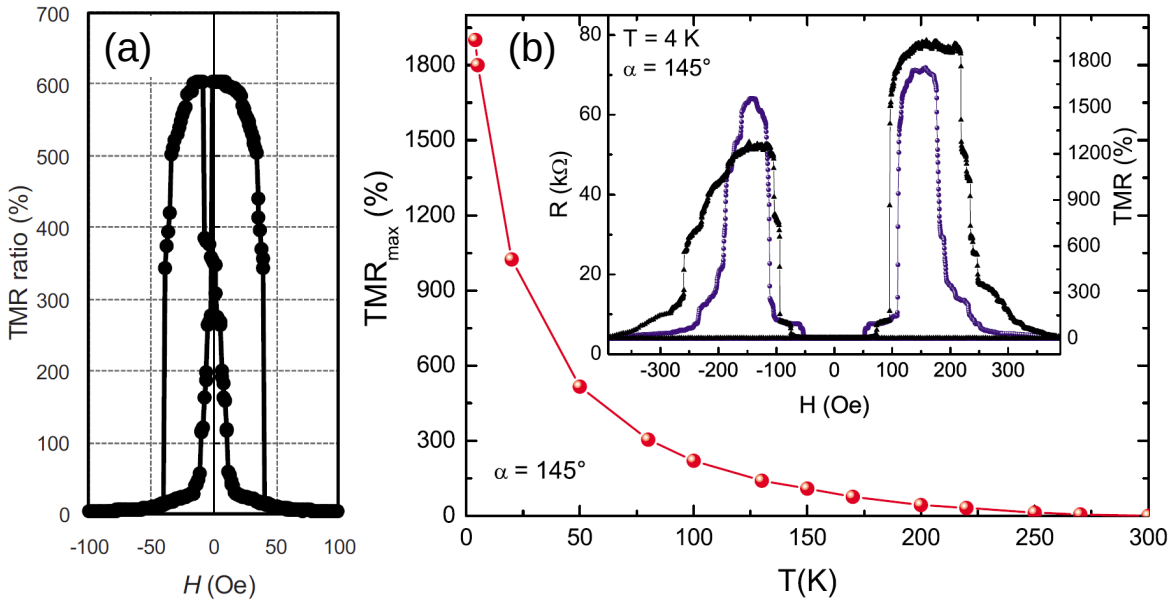

Fig. 4.36: (a) Tunnel magnetoresistance vs. applied magnetic field for a CoFeB/MgO/CoFeB tunnel junction at 300 K; from [Ikeda et al., 2008]. (b) TMR effect in a LSMO/STO/LSMO tunnel junction. Main graph shows the T dependence of the maximum TMR value. Inset shows resistance R and TMR vs. H; from [Werner et al., 2011].

(e.g. Sr_2FeMoO_6 mit $T_C = 421\,K$ or Sr_2FeReO_6 with $T_C \approx 540\,K$),
- Heusler alloys, e.g.
NiMnSb ($T_C = 728\,K$), PtMnSBb ($T_C = 572\,K$) and Co_2MnSi ($T_C = 985\,K$)

Steady improvement of the properties of the materials and interfaces, and choice of suitable barrier materials ($SrTiO_3$, AlO_x, TiO_x, MgO) [Zhu and Park, 2006]
→ further increase of the TMR values with, up to now, highest values of
$TMR \sim 600\,\%$ at $300\,K$ in CoFeB/MgO/CoFeB [Ikeda et al., 2008]; see Fig. 4.36(a).

4.6 List of Original Literature

[ILL, 2016] (2016). ILL News 65 – Special issue Haldane. Institut Laue-Langevin (Grenoble); https://www.ill.eu/fileadmin/users_files/ILL_News/65/ILLnews_65-Haldane.pdf.

[Baibich et al., 1988] Baibich, M. N., Broto, J. M., Fert, A., Dau, F. N. V., Petroff, F., Etienne, P., Creuzet, G., Friederich, A., and Chazelas, J. (1988). Giant magnetoresistance of (001)Fe/(001)Cr magnetic superlattices. Phys. Rev. Lett., 61:2472–2475.

[Barnas et al., 1990] Barnas, J., Fuss, A., Camley, R. E., Grünberg, P., and Zinn, W. (1990). Novel magnetoresistance effect in layered magnetic structures: Theory and experiment. Phys. Rev. B, 42:8110.

[Bartolomé et al., 2014] Bartolomé, J., Luis, F., and Fernández, J. F., editors (2014). Molecular Magnets. Physics and Applications. Springer-Verlag, Berlin Heidelberg.

[Binasch et al., 1989] Binasch, G., Grünberg, P., Saurenbach, F., and Zinn, W. (1989). Enhanced magnetoresistance in layered magnetic structures with antiferromagnetic interlayer exchange. Phys. Rev. B, 39:4828–4830.

[Bode et al., 2004] Bode, M., Pietzsch, O., Kubetzka, A., and Wiesendanger, R. (2004). Shape-dependent thermal switching behavior of superparamagnetic nanoislands. Phys. Rev. Lett., 92:067201.

[Brown, 1940] Brown, W. F. (1940). Theory of the approach to magnetic saturation. Phys. Rev., 58:736–743.

[Brown, 1963] Brown, W. F. (1963). Thermal fluctuations of a single-domain particle. Phys. Rev., 130:1677–1686.

[Buchter et al., 2013] Buchter, A., Nagel, J., Rüffer, D., Xue, F., Weber, D. P., Kieler, O. F., Weimann, T., Kohlmann, J., Zorin, A. B., Russo-Averchi, E., Huber, R., Berberich, P., Fontcuberta i Morral, A., Kemmler, M., Kleiner, R., Koelle, D., Grundler, D., and Poggio, M. (2013). Reversal mechanism of an individual Ni nanotube simultaneously studied by torque and SQUID magnetometry. Phys. Rev. Lett., 111:067202.

[Cowley and Rosensweig, 1967] Cowley, M. D. and Rosensweig, R. E. (1967). J. Fluid Mech., 30:671.

[Datta and Das, 1990] Datta, S. and Das, B. (1990). Electronic analog of the electro-optic modulator. Appl. Phys. Lett., 56:665.

[Degen, 2008] Degen, C. (2008). Nanoscale magnetometry: Microscopy with single spins. Nature Nanotechnol., 3:643–644.

[Dieny et al., 1991] Dieny, B., Speriosu, V. S., Parkin, S. S. P., Gurney, B. A., Wilhoit, D. R., and Mauri, D. (1991). Giant magnetoresistive in soft ferromagnetic multilayers. Phys. Rev. B, 43:1297.

[Fruchart, 2015] Fruchart, O. (2015). Lecture notes on nanomagnetism; htpp://perso.neel.cnrs.fr/olivier.fruchart/.

[Gross and Marx, 2012] Gross, R. and Marx, A. (2012). Festköperphysik. Oldenbourg Verlag, München.

[Grünberg, 1995] Grünberg, P. (1995). Magnetische Schichtstrukturen: Zwischenaustauschkopplung und Riesenmagnetowiderstandseffekt. IFF-Bulletin, 47:10.

[Guimarães, 2009] Guimarães, A. P. (2009). Principles of Nanomagnetism. Springer-Verlag, Berlin Heidelberg.

[Hornyak et al., 2009] Hornyak, G. L., Moore, J. J., Tibbals, H. F., and Dutta, J. (2009). Fundamentals of Nanotechnology. CRC Press, London, New York.

[Hubert and Schäfer, 1998] Hubert, A. and Schäfer, R. (1998). Magnetic Domains: The Analysis of Magnetic Microstructures. Springer-Verlag, Berlin.

[Ikeda et al., 2008] Ikeda, S., Hayakawa, J., Ashizawa, Y., Lee, Y. M., Miura, K., Hasegawa, H., Tsunoda, M., Matsukura, F., and Ohno, H. (2008). Tunnel magnetoresistance of 604 % at 300 K by suppression of Ta diffusion in CoFeB/MgO/CoFeB pseudo-spin-valves annealed at high temperature. Appl. Phys. Lett., 93:082508.

[Julliere, 1975] Julliere, M. (1975). Tunneling between ferromagnetic films. Phys. Lett., 54A:225–226.

[Kasuya, 1956] Kasuya, T. (1956). A theory of metallic ferro- and antiferromagnetism on Zener's model. Prog. Theor. Phys., 16:45–57.

[Kleibert and Nolting, 2013] Kleibert, A. and Nolting, F. (2013). Magnetische nanowelt. Physik Journal, 12:27–32.

[Lu and an F. Schüth, 2007] Lu, A.-H. and an F. Schüth, E. L. S. (2007). Magnetic nanoparticles: Synthesis, protection, functionalization, and application. Angew. Chem. Int. Ed., 46:1222–1244.

[Martínez-Pérez and Koelle, 2017] Martínez-Pérez, M. J. and Koelle, D. (2017). NanoSQUDs: Basics & recent advances. Phys. Sci. Rev., 2:20175001. arXiv:1609.06182v2 [cond-mat.supr-con].

[Mermin and Wagner, 1966] Mermin, N. D. and Wagner, H. (1966). Absence of ferromagnetism or antiferromagnetism in one- or two-dimensional isotropic Heisenberg models. Phys. Rev. Lett., 17:1133–1136.

[Meservey et al., 1970] Meservey, R., Tedrow, P. M., and Fulde, P. (1970). Magnetic field splitting of the quasiparticle states in superconducting aluminium films. Phys. Rev. Lett., 25:1270.

[Monsma et al., 1995] Monsma, D. J., Lodder, J. C., Popma, T. J. A., and Dieny, B. (1995). Perpendicular hot electron spin-valve effect in a new magnetic field sensor: The spin-valve transistor. Phys. Rev. Lett., 74:5260.

[Moodera et al., 1995] Moodera, J. S., Kinder, L. R., Wong, T. M., and Meservey, R. (1995). Large magnetoresistance at room temperature in ferromagnetic thin film tunnel junctions. Phys. Rev. Lett., 74:3273.

[Moodera et al., 1999] Moodera, J. S., Nassar, J., and Mathon, G. (1999). Spin-tunneling in ferromagnetic junctions. Annu. Rev. Mater. Sci., 29:381–432.

[Moodera et al., 1998] Moodera, J. S., Nowak, J., and de Veerdonk, R. J. M. V. (1998). Interface magnetism and spin wave scattering in ferromagnet-insulator-ferromagnet tunnel junctions. Phys. Rev. Lett., 80:2941.

[Mott, 1964] Mott, N. F. (1964). Electrons in transtion metals. Adv. Phys., 13:325–422.

[Néel, 1947] Néel, L. (1947). C. R. Acad. Science, 224:1550.

[Néel, 1953] Néel, L. (1953). L'anisotropie superficielle des substances ferromagnétiques. CR Acad. Sci. Paris, 237:1468–1470.

[Néel, 1954] Néel, L. (1954). Anisotropie magnétique superficielle et surstructures d'orientation. J. Phys. Radium, 15:225–239.

[Poggio and Degen, 2010] Poggio, M. and Degen, C. L. (2010). Force-detected nuclear magnetic resonance: recent advances and future challenges. Nanotechnology, 21:342001.

[Richter, 2008] Richter, R. (2008). Flüssige magnetische gebirge. Physik Journal, 7:39–44.

[Ruderman and Kittel, 1954] Ruderman, M. A. and Kittel, C. (1954). Indirect exchange coupling of nuclear magnetic moments by conduction electrons. Phys. Rev., 96:99–102.

[Rugar et al., 2004] Rugar, D., Budakian, R., Mamin, H. J., and Chui, B. W. (2004). Single spin detection by magnetic resonance force microscopy. Nature, 430:329–332.

[Schneider et al., 1990] Schneider, C. M., Bressler, P., Schuster, P., Kirschner, J., de Miguel, J. J., and Miranda, R. (1990). Curie temperature of ultrathin films of fcc-cobalt epitaxially grown on atomically flat Cu(100) surfaces. Phys. Rev. Lett., 64:1059–1062.

[Schreiber et al., 1995] Schreiber, F., Frait, Z., Zeidler, T., Metoki, N., Donner, W., Zabel, H., and Pelzl, J. (1995). Strong anisotropies in MBE-grown Co/Cr(001): Ferromagnetic-resonance and magneto-optical Kerr-effect studies. Phys. Rev. B, 51:2920–2929.

[Schuller, 2004] Schuller, I. K. (2004). Unusual phenomena in exchange-biased nanostructures. Mater. Res. Bull., 29:642–646.

[Schwarz et al., 2015] Schwarz, T., Wölbing, R., Reiche, C. F., Müller, B., Martínez-Pérez, M. J., Mühl, T., Büchner, B., Kleiner, R., and Koelle, D. (2015). Low-noise $YBa_2Cu_3O_7$ nano-SQUIDs for performing magnetization-reversal measurements on magnetic nanoparticles. Phys. Rev. Appl., 3:044011.

[Stoner and Wohlfarth, 1948] Stoner, E. C. and Wohlfarth, E. P. (1948). A mechanism of magnetic hysteresis in heterogeneous alloys. Philos. Trans. R. Soc. London, Ser. A, 240(826):599–642. reprinted in IEEE Trans. Magn. MAG **27**, 3475 (1991).

[Tedrow and Meservey, 1971] Tedrow, P. M. and Meservey, R. (1971). Spin-dependent tunneling into ferromagnetic nickel. Phys. Rev. Lett., 26:192.

[Van Santen and Jonker, 1950] Van Santen, J. H. and Jonker, G. H. (1950). Electrical conductivity of ferromagnetic compounds of manganese with perovskite structure. Physica, 16:599–600.

[von Helmolt et al., 1993] von Helmolt, R., Wecker, J., Holzapfel, B., Schultz, L., and Samwer, K. (1993). Giant negative magnetoresistance in perovskitelike $La_{2/3}Ba_{1/3}MnO_x$ ferromagnetic thin films. Phys. Rev. Lett., 71:2331–2334.

[Werner et al., 2011] Werner, R., Petrov, A. Y., no, L. A. M., Kleiner, R., Koelle, D., and Davidson, B. A. (2011). Improved tunneling magnetoresistance at low temperature in manganite junctions grown by molecular beam epitaxy. Appl. Phys. Lett., 98:162505.

[Wernsdorfer, 2001] Wernsdorfer, W. (2001). Classical and quantum magnetization reversal studied in nanometersized particles and clusters. Adv. Chem. Phys., 118:99–190.

[Wernsdorfer, 2009] Wernsdorfer, W. (2009). From micro- to nano-SQUIDs: applications to nanomagnetism. Supercond. Sci. Technol., 22:064013.

[Wood, 2009] Wood, R. (2009). Future hard disk drive systems. J. Magn. Magn. Mater., 321:555–561.

[Yosida, 1957] Yosida, K. (1957). Magnetic properties of Cu-Mn alloys. Phys. Rev., 106:893–898.

[Zhu and Park, 2006] Zhu, J.-G. J. and Park, C. (2006). Magnetic tunnel junctions. Materials Today, 9(11):36–45.

4.7 Recommendations for Further Reading

- Stefan Blügel, Thomas Brückel, Claus M. Schneider (Eds.), *Magnetism goes Nano*, Lecture Manuscripts of the 36^{th} Spring School of the Institute of Solid State Research, Volume 26 in the series *Matter and Material*, Forschungszentrum Jülich, 2005
- Olivier Fruchart, *Lecture Notes on Nanomagnetism*, Institut Néel (CNRS & Univ. Grenoble), Oct. 2018; http://fruchart.eu/olivier/lectures/nanomagnetism-2018-09-17.pdf
- Gabor L. Hornyak, John J. Moore, Harry F. Tibbals, Joydeep Dutta, *Fundamentals of Nanotechnology*, CRC Press (London, New York), 2009.
- Alberto P. Guimarães, *Principles of Nanomagnetism*, Springer-Verlag (2009)

Literature on MNPs and SMMs:

- Juan Bartolomé, Fernando Luis, Julio F. Fernandéz, *Molecular Magnets: Physics and Applications*, Springer-Verlag (Berlin, Heidelberg), 2014
- Chris Binns, *Tutorial Section on Nanomagnetism*, in *Frontiers of Nanoscience, Vol. 6: Nanomagnetism: Fundamentals and Applications*, Elsevier (2014)
- Wolfgang Wernsdorfer, *Classical and quantum magnetization reversal studied in nanometer-sized particles and clusters*, Adv. Chem. Phys. **118**, 99 (2001); arXiv:cond-mat/0101104.

Literature on spintronics (incl. GMR, TMR):

- R. Gross, A. Marx, *Spinelektronik* (in German); lecture notes on Spin Electronics, Walther-Meissner-Institut (WMI), Garching (2004), http://www.wmi.badw.de/teaching/lecture-notes.
- R. Meservey, P. M. Tedrow, *Spin-polarized electron tunneling*, Phys. Rep. **238**, 173-243 (1994)
- J. S. Moodera, J. Nassar, G. Mathon, *Spin-tunneling in ferromagnetic junctions*, Annu. Rev. Mater. Sci. **29**, 381-432 (1999)
- E. L. Wolf, *Principles of electron tunneling spectroscopy*, Oxford Univ. Press (New York), 1985